CHAPTER IV
RESULTS AND DISCUSSION

The first section of this chapter focuses on the density of five pure ionic liquids and the influence of temperature. Section 4.2 discusses the experimental solubility of CO_2 in the studied ionic liquids. The effects of temperature, pressure, and structure of cations and anions are discussed. Moreover, the comparison between the experimental CO_2 solubility data in the ionic liquids and those published in literature is also presented. Section 4.3 provides information regarding the normal boiling temperature, critical properties and acentric factor estimation as well as consistency test on the density. In addition, this section contains details on the thermodynamic models used to correlate the experimental CO_2 solubility data including well-known equations of state, such as the Peng-Robinson (PR-EoS), Redlich-Kwong-Soave (SRK-EoS), and the Redlich-Kwong-Soave (SRK) with quadratic mixing rules, and finally the Non-Random Two-Liquid (NRTL) activity coefficient model. The Henry's law constants and enthalpies and entropies of absorption for CO_2 in different ionic liquids are discussed in the last section.
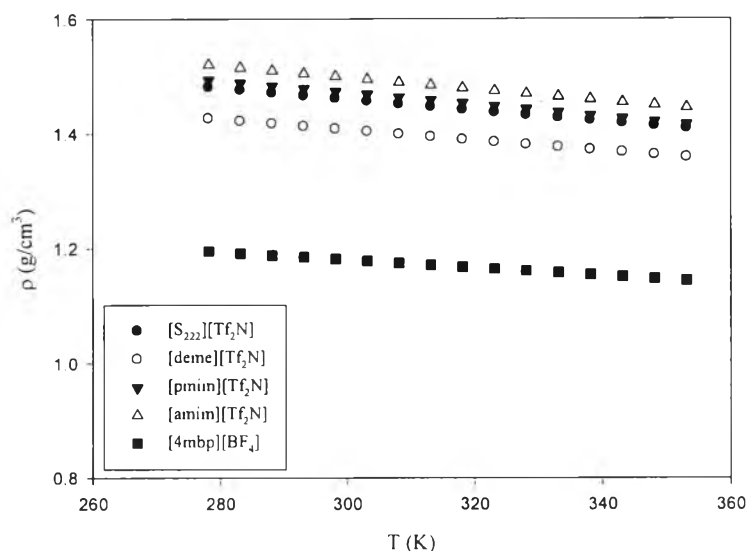
4.1 Density of Pure Ionic Liquids

The densities of triethylsulfonium bis(trifluoromethylsulfonyl)imide ($[S_{222}][Tf_2N]$), diethylmethyl(2-methoxyethyl)ammonium bis(trifluoromethyl sulfonyl)imide ($[deme][Tf_2N]$), 1-propyl-3-methylimidazolium bis(trifluoromethyl sulfonyl)imide ($[pmim][Tf_2N]$), 1-allyl-3-methylimidazolium bis(trifluoromethyl sulfonyl)imide ($[amim][Tf_2N]$), and 1-butyl-4-methylpyridinium tetrafluoroborate ($[4mbp][BF_4]$) were measured at atmospheric pressure as a function of temperature ranging from 278.15 K to 353.15 K. The ionic liquids remained liquid over the whole range of temperature. The experimental densities are presented in Table 4.1. In the temperature interval from 278.15 K to 353.15 K, the densities of all investigated ionic liquids decreased linearly with an increase in temperature as depicted in Figure 4.1. Of the ionic liquids based on the bis(trifluoromethylsulfonyl)imide anion ($[Tf_2N^-]$), $[amim][Tf_2N]$ apparently has the highest density values over the whole

range of studied temperatures. At 298.15 K, the density of [amim][Tf$_2$N] is 1.49974 g/cm^3. Meanwhile, [S$_{222}$][Tf$_2$N], [deme][Tf$_2$N] and [pmim][Tf$_2$N] had the lowest density values. The densities of [S$_{222}$][Tf$_2$N], [deme][Tf$_2$N] and [pmim][Tf$_2$N] are 1.46118, 1.40809 and 1.47337, respectively. Recently, Gómez *et al.* discussed the physical properties of [pmim][Tf$_2$N] and its density in (Gómez *et al.*, 2012). The density value of [pmim][Tf$_2$N] at 298.15 K was reported to be 1.47444 g/cm^3, which differs from our experimental result, but the two solvents had different purities and water contents. The ionic liquid [4mbp][BF$_4$] presents far lower density than other studied ionic liquids with a value of 1.18103 g/cm^3 at 298.15 K. The densities of the investigated ionic liquids diminished in the following sequence: [amim][Tf$_2$N] > [pmim][Tf$_2$N] > [S$_{222}$][Tf$_2$N] > [deme][Tf$_2$N] > [4mbp][BF$_4$]. The temperature-dependent correlations of density for each ionic liquid are expressed as a linear function with a correlation coefficient R^2 > 0.999, as shown in Table 4.2. The average absolute deviations (AADs) between the experimental and calculated densities of [S$_{222}$][Tf$_2$N], [deme][Tf$_2$N], [pmim][Tf$_2$N], [amim][Tf$_2$N], and [4mbp][BF$_4$] are 0.13, 0.03, 0.08, 0.02 and 0.08 %, respectively.

Table 4.1 Experimental densities of the five ionic liquids measured at 1.01325 bar

T (K)	ρ (g/cm^3)				
	[S$_{222}$][Tf$_2$N]	[deme][Tf$_2$N]	[pmim][Tf$_2$N]	[amim][Tf$_2$N]	[4mbp][BF$_4$]
278.15	1.48082	1.42664	1.49344	1.52037	1.19503
283.15	1.47589	1.42201	1.48842	1.51520	1.19152
288.15	1.47096	1.41736	1.48339	1.51002	1.18799
293.15	1.46606	1.41271	1.47838	1.50487	1.18447
298.15	1.46118	1.40809	1.47337	1.49974	1.18103
303.15	1.45633	1.40347	1.46839	1.49464	1.17766
308.15	1.45151	1.39888	1.46342	1.48956	1.17428
313.15	1.44671	1.39430	1.45844	1.48452	1.17090
318.15	1.44193	1.38974	1.45343	1.47950	1.16752
323.15	1.43718	1.38520	1.44828	1.47452	1.16415
328.15	1.43245	1.38069	1.44297	1.46955	1.16081
333.15	1.42775	1.37619	1.43756	1.46461	1.15746
338.15	1.42307	1.37171	1.43189	1.45969	1.15414
343.15	1.41841	1.36726	1.42672	1.45480	1.15083
348.15	1.41377	1.36282	1.42143	1.44994	1.14753
353.15	1.40916	1.35840	1.41638	1.44510	1.14425

Figure 4.1 Liquid density of the studied ionic liquids at temperatures ranging from 278.15 K to 353.15 K: ●, [S$_{222}$][Tf$_2$N]; ○, [deme][Tf$_2$N]; ▼, [pmim][Tf$_2$N]; △, [amim][Tf$_2$N]; ■, [4mbp][BF$_4$].

Table 4.2 Temperature-dependent density correlations for the studied ionic liquids

| Ionic liquids	Density (g/cm^3)	AAD (%)
[S$_{222}$][Tf$_2$N]	ρ (g/cm^3) = 1.4852-0.001×[T(K)-273.15]	0.13
[deme][Tf$_2$N]	ρ (g/cm^3) = 1.4309-0.0009×[T(K)-273.15]	0.03
[pmim][Tf$_2$N]	ρ (g/cm^3) = 1.4991-0.001×[T(K)-273.15]	0.08
[amim][Tf$_2$N]	ρ (g/cm^3) = 1.525-0.001×[T(K)-273.15]	0.02
[4mbp][BF$_4$]	ρ (g/cm^3) = 1.1981-0.0007×[T(K)-273.15]	0.08

4.2 Solubility of Carbon Dioxide

4.2.1 Experimental Solubility Isotherms

Determination of gas solubility plays an important role in ionic liquid selection in order to explore novel ionic liquids as potential solvents for CO_2 absorption. This work focuses mainly on ionic liquids exhibiting physical absorption

with CO_2. Experimental solubility isotherms of five ionic liquids including [S_{222}][Tf_2N], [deme][Tf_2N], [pmim][Tf_2N], [amim][Tf_2N], and [4mbp][BF_4] were measured at 313.15, 323.15 and 333.15 K at different pressures under 20 bar using an Intelligent Gravimetric Analyzer (IGA-003) manufactured by Hiden Isochema. Solubility measurement of CO_2 in [bmim][PF_6] at 323.15 K was carried out to validate the apparatus and the measurement method by comparing the results to solubility data existing in the literature. The solubility data of CO_2 in [bmim][PF_6] at 323.15 K is comparable to the available values published by Shiflett and Yokozeki (2005) and Anthony *et al.* (2002) as shown in Figure 4.2. The AADs of the measured and reported solubilities at 323.15 K are 4 and 12 %, respectively.

Experimental solubility data for [S_{222}][Tf_2N] (1) + CO_2 (2), [deme][Tf_2N] (1) + CO_2 (2), [pmim][Tf_2N] (1) + CO_2 (2), [amim][Tf_2N] (1) + CO_2 (2) and [4mbp][BF_4] (1) + CO_2 (2) systems at 313.15, 323.15 and 333.15 K are presented in Table 4.3. The solubility results are given in terms of the percentage of mole fraction of CO_2 dissolved in the ionic liquids.
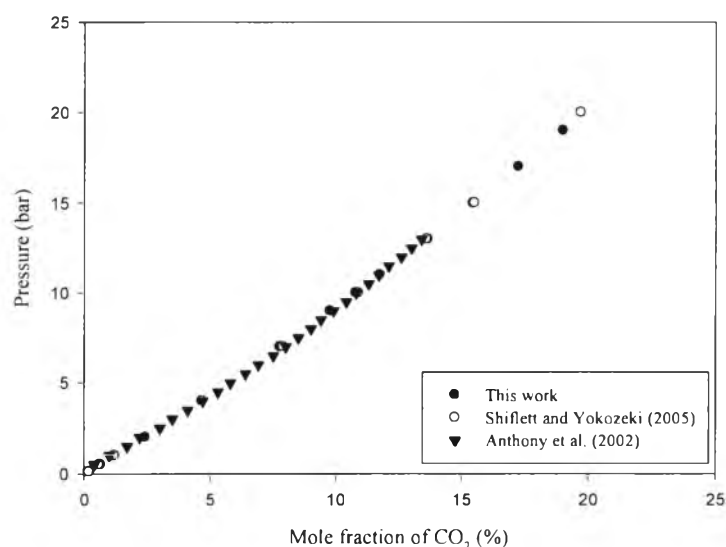
Figure 4.2 Absorption of CO_2 in [bmim][PF_6] at 323.15 K compared to the solubility data obtained in literature: ●, this work; ○, Shiflett and Yokozeki (2005); ▼, Anthony *et al.* (2002).

Table 4.3 Experimental solubility (P, T, x) data for [S$_{222}$][Tf$_2$N] (1) + CO$_2$ (2), [deme][Tf$_2$N] (1) + CO$_2$ (2), [pmim][Tf$_2$N] (1) + CO$_2$ (2), [amim][Tf$_2$N] (1) + CO$_2$ (2) and [4mbp][BF$_4$] (1) + CO$_2$ (2) systems at 313.15, 323.15 and 333.15 K

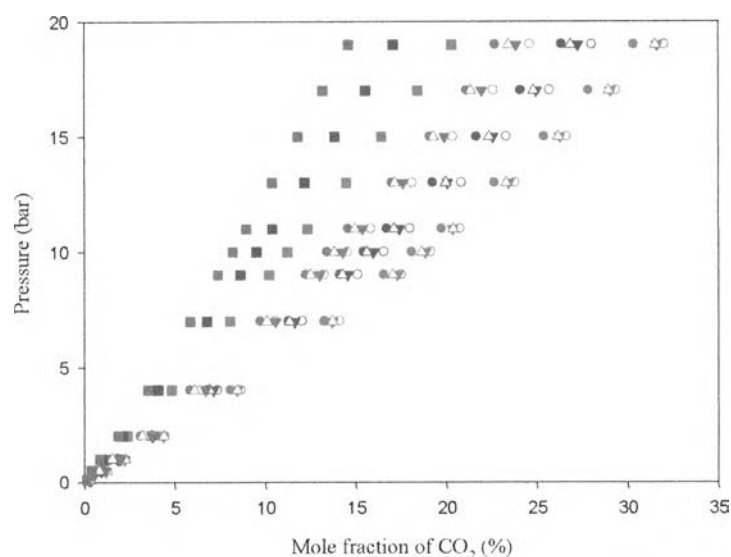| [S$_{222}$][Tf$_2$N]		[deme][Tf$_2$N]		[pmim][Tf$_2$N]		[amim][Tf$_2$N]		[4mbp][BF$_4$]	
P (bar)	100x$_2$	P (bar)	100x$_2$	P (bar)	100x$_2$	P (bar)	100x$_2$	P (bar)	100x$_2$
At 313.15 K									
0.0947	0.24	0.1011	0.25	0.0993	0.27	0.0997	0.27	0.1018	0.11
0.5000	1.08	0.4991	1.19	0.5018	1.18	0.4999	1.20	0.4992	0.57
0.9991	2.05	0.9961	2.23	1.0007	2.20	0.9987	2.22	0.9990	1.13
2.0019	4.12	1.9963	4.43	1.9991	4.33	1.9994	4.36	2.0008	2.37
3.9968	8.06	3.9981	8.65	3.9989	8.41	3.9998	8.43	3.9984	4.81
6.9983	13.24	7.0009	14.09	6.9987	13.68	7.0016	13.68	7.0007	8.02
8.9979	16.52	8.9982	17.49	8.9995	17.27	9.0003	17.01	8.9983	10.19
9.9963	18.07	9.9987	19.12	9.9980	18.81	10.0000	18.60	9.9979	11.20
10.9983	19.72	10.9993	20.74	11.0003	20.33	10.9997	20.34	10.9996	12.31
12.9981	22.63	12.9977	23.80	12.9985	23.42	13.0018	23.25	12.9985	14.45
15.0000	25.39	14.9996	26.63	14.9985	26.24	14.9969	26.14	14.9989	16.40
16.9999	27.84	17.0007	29.37	16.9998	29.03	16.9979	28.94	17.0042	18.38
18.9978	30.33	18.9982	32.02	18.9982	31.60	18.9949	31.50	18.9984	20.28
At 323.15 K									
0.1027	0.20	0.0985	0.23	0.0998	0.23	0.0995	0.21	0.0954	0.10
0.5002	0.84	0.4992	0.99	0.5000	0.92	0.4996	0.86	0.4983	0.50
0.9990	1.69	0.9999	1.91	0.9985	1.82	0.9987	1.77	0.9991	1.01
1.9982	3.52	1.9998	3.87	2.0002	3.74	2.0014	3.69	2.0014	2.10
3.9988	6.80	3.9986	7.36	3.9996	7.11	3.9986	6.91	3.9994	4.09
6.9979	11.27	7.0020	12.03	6.9983	11.60	6.9991	11.32	6.9984	6.76
8.9993	14.12	9.0001	15.11	8.9994	14.52	8.9998	14.22	8.9998	8.61
9.9998	15.43	10.0002	16.56	9.9980	15.95	9.9996	15.59	9.9982	9.50
10.9993	16.71	10.9988	18.01	10.9989	17.37	10.9999	17.08	10.9992	10.37
12.9974	19.24	12.9994	20.83	13.0003	20.04	12.9977	19.94	12.9979	12.16

Table 4.3 Experimental solubility (P, T, x) data for [S$_{222}$][Tf$_2$N] (1) + CO$_2$ (2), [deme][Tf$_2$N] (1) + CO$_2$ (2), [pmim][Tf$_2$N] (1) + CO$_2$ (2), [amim][Tf$_2$N] (1) + CO$_2$ (2) and [4mbp][BF$_4$] (1) + CO$_2$ (2) systems at 313.15, 323.15 and 333.15 K (cont.)

[S$_{222}$][Tf$_2$N]		[deme][Tf$_2$N]		[pmim][Tf$_2$N]		[amim][Tf$_2$N]		[4mbp][BF$_4$]	
P (bar)	100x$_2$	P (bar)	100x$_2$	P (bar)	100x$_2$	P (bar)	100x$_2$	P (bar)	100x$_2$
15.0025	21.67	14.9992	23.32	14.9989	22.55	14.9993	22.33	14.9971	13.83
16.9990	24.10	17.0075	25.71	16.9984	24.96	16.9990	24.81	16.9990	15.52
19.0062	26.37	18.9985	28.05	19.0025	27.24	18.9978	26.84	19.0006	17.06
At 333.15 K									
0.1014	0.21	0.0987	0.30	0.0990	0.37	0.1005	0.24	0.1030	0.10
0.4984	0.73	0.4991	0.89	0.5003	1.13	0.4990	0.78	0.4994	0.39
0.9989	1.52	0.9987	1.66	0.9998	1.97	0.9985	1.51	0.9986	0.85
1.9986	3.09	1.9982	3.42	1.9994	3.72	1.9991	3.17	2.0016	1.86
3.9973	5.84	3.9984	6.44	3.9990	6.66	3.9977	6.06	3.9984	3.50
6.9975	9.72	6.9947	10.55	6.9963	10.55	7.0008	10.06	6.9985	5.85
9.0006	12.23	8.9965	13.25	8.9982	12.98	8.9995	12.47	9.0003	7.37
9.9974	13.41	9.9986	14.55	9.9992	14.24	10.0000	13.79	9.9988	8.19
10.9980	14.55	11.0043	15.83	11.0005	15.35	11.0001	14.91	10.9987	8.95
12.9975	16.98	12.9989	18.12	12.9986	17.58	12.9970	17.12	12.9967	10.35
14.9975	19.08	14.9976	20.35	15.0004	19.86	14.9987	19.26	15.0009	11.77
16.9979	21.11	17.0030	22.60	16.9983	21.91	17.0000	21.32	17.0017	13.16
18.9981	22.69	19.0044	24.62	18.9917	23.82	18.9948	23.40	18.9985	14.58

4.2.2 Effects of Temperature and Pressure

It has been reported that the solubility of CO$_2$ in ionic liquids can be dramatically affected by temperature and pressure. To clearly understand the influence in temperature and pressure on the solubility of CO$_2$, graphical representation of our solubility data in Figure 4.3 is displayed as a function of pressure at different temperatures for all of the studied ionic liquids. The solubility decreases as temperature increases and pressure decreases for all of the ionic liquids

studied. At the same temperature, trends of the CO_2 solubility in the ionic liquids are likely to decrease in this following order: [deme][Tf_2N] > [pmim][Tf_2N] > [amim][Tf_2N] > [S_{222}][Tf_2N]. When the pressure increases, the solubility of CO_2 linearly increases at low pressure and further increases nonlinearly at higher pressure.
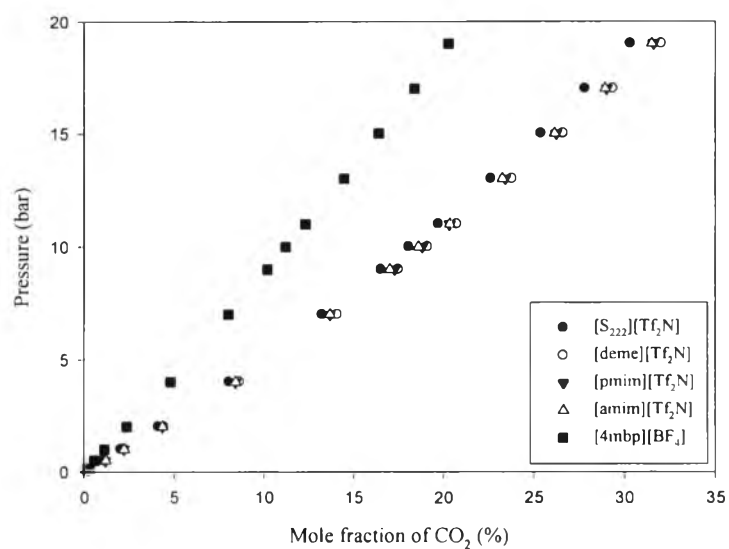

Figure 4.3 Comparison of measured isothermal solubility data of CO_2 in different ionic liquids: ●, [S_{222}][Tf_2N]; ○, [deme][Tf_2N]; ▼, [pmim][Tf_2N]; △, [amim][Tf_2N]; ■, [4mbp][BF_4]; red, at 313.15 K; blue, at 323.15 K; green, at 333.15 K.

4.2.3 Effects of Cations and Anions

Structural variation of cations and anions of ionic liquids is an important factor that has a direct impact on the solubility of CO_2. The effect of the cation of the ionic liquids on the CO_2 solubility is studied by comparing the solubility with a similar anion but with different cations. The comparisons of experimentally measured solubilities of CO_2 in the ionic liquids at each temperature are illustrated in Figure 4.4-4.6. Considering ionic liquids based on the [Tf_2N^-] anion, the ionic liquid with ammonium-based cation, [deme][Tf_2N], apparently shows the highest solubility of CO_2. The mole fractions of CO_2 in [deme][Tf_2N] at a

pressure of 19 bar and temperatures of 313.15, 323.15 and 333.15 K are 32.02, 28.05 and 24.62 %, respectively. However, the solubility of CO_2 in [deme][Tf_2N] is comparable to other studied imidazolium-based ionic liquids including [pmim][Tf_2N] and [amim][Tf_2N]. At 19 bar pressure, the values of mole fraction of CO_2 in [pmim][Tf_2N] at 313.15, 323.15 and 333.15 K are 31.60, 27.24 and 23.82 %, and those in [amim][Tf_2N] are 31.50, 26.84 and 23.40 %, respectively. The cation structure of [amim][Tf_2N] contains a double bond on the C_3 alkyl position, whereas [pmim][Tf_2N] contains only a single bond on the alkyl chain. Between the two ionic liquids with C_3 alkyl chain, [pmim][Tf_2N] exhibits higher CO_2 solubility than [amim][Tf_2N]. According to Sumon and Henni, the polarity of ionic liquids which reflects the overall solvation capacity due to a number of solute-solvent interactions can qualitatively describe the trend of the solubility of CO_2 in ionic liquids. They also indicated that Henry's law constant of CO_2 in ionic liquids decreased as polarity of ionic liquids decreased (Sumon and Henni, 2011). Therefore, we can imply that the solubility of CO_2 in ionic liquids is enhanced with a decrease in their polarity. In terms of dualistic theory, double bonds were explained to be polar, likewise, the assumption of polarity accounted for the reactivity of double bonds (Carothers, 1924). In conclusion, the presence of a double bond on the alkyl chain of the cation of [amim][Tf_2N] which leads to higher polarity of the ionic liquid apparently lowers the solubility of CO_2. To the best of our knowledge, CO_2 is considered to be nonpolar. The explanation given above confirms our observation that nonpolar CO_2 is more soluble into the less polar ionic liquid which is [pmim][Tf_2N] which therefore exhibiting superior CO_2 solubility.

Figure 4.4 Comparison of measured isothermal solubility data of CO_2 in different ionic liquids at 313.15 K: ●, $[S_{222}][Tf_2N]$; ○, $[deme][Tf_2N]$; ▼, $[pmim][Tf_2N]$; △, $[amim][Tf_2N]$; ■, $[4mbp][BF_4]$.
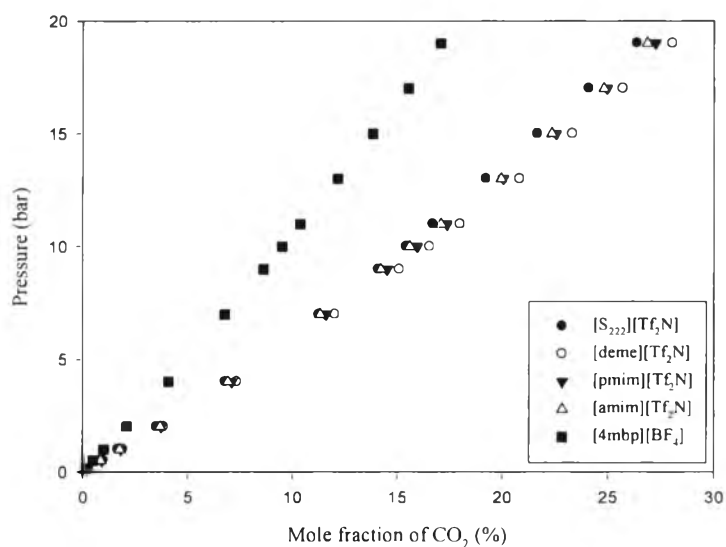
Figure 4.5 Comparison of measured isothermal solubility data of CO_2 in different ionic liquids at 323.15 K: ●, $[S_{222}][Tf_2N]$; ○, $[deme][Tf_2N]$; ▼, $[pmim][Tf_2N]$; △, $[amim][Tf_2N]$; ■, $[4mbp][BF_4]$.
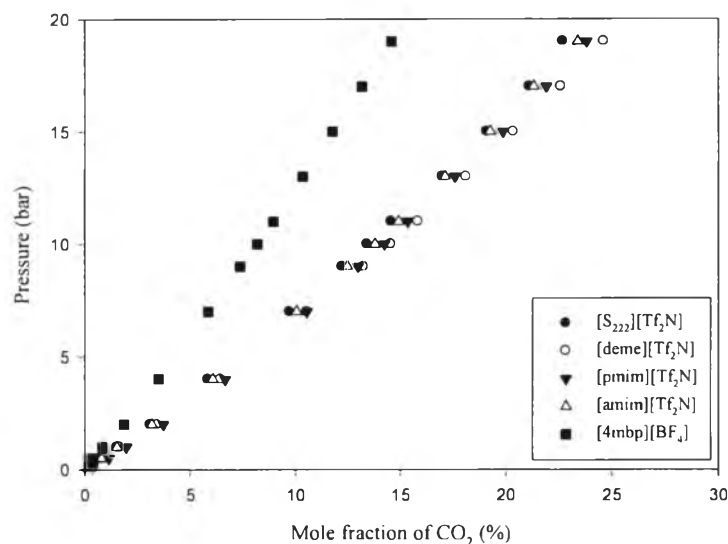
Figure 4.6 Comparison of measured isothermal solubility data of CO_2 in different ionic liquids at 333.15 K: •, [S$_{222}$][Tf$_2$N]; ○, [deme][Tf$_2$N]; ▼, [pmim][Tf$_2$N]; Δ, [amim][Tf$_2$N]; ■, [4mbp][BF$_4$].

There are a number of publications regarding the solubility of CO_2 in a variety of ionic liquids: CO_2 + 2-(2-hydroxy ethoxy)-ammonium formate (HEAF) (Yuan *et al.*, 2007), CO_2 + 2-hydroxy ethylammonium lactate (HEL) (Yuan *et al.*, 2007), CO_2 + tri-(2-hydroxy ethyl)-ammonium acetate (THEAA) (Yuan *et al.*, 2007), CO_2 + 2-hydroxy ethylammonium formate (HEF) (Yuan *et al.*, 2007), CO_2 + 2-(2-hydroxy ethoxy)-ammonium lactate (HEAL) (Yuan *et al.*, 2007), CO_2 + 2-hydroxy ethylammonium acetate (HEA) (Yuan *et al.*, 2007), CO_2 + tri-(2-hydroxy ethyl)-ammonium lactate (THEAL) (Yuan *et al.*, 2007), CO_2 + 2-(2-hydroxy ethoxy)-ammonium acetate (HEAA) (Yuan *et al.*, 2007), CO_2 + 1-butyl-3-methylimidazolium tetrafluoroborate ([bmim][BF$_4$]) (Shiflett and Yokozeki, 2005), CO_2 + 1-butyl-3-methylimidazolium hexafluorophosphate ([bmim][PF$_6$]) (Shiflett and Yokozeki, 2005), CO_2 + 1-butyl-3-methylimidazolium bis(trifluoromethylsulfonyl)imide ([bmim][Tf$_2$N]) (Anthony *et al.*, 2005), CO_2 + 1-hexyl-3-methylimidazolium bis(trifluoromethylsulfonyl)imide ([hmim][Tf$_2$N]) (Shiflett and Yokozeki, 2007), CO_2 + 1-butyl-1-methylpyrrolidinium

tris(pentafluoroethyl)trifluorophosphate ([bmpyrr][eFAP]) (Zhang *et al.*, 2008), CO_2 + 1-hexyl-3-methylimidazolium tris(pentafluoroethyl)trifluorophosphate ([hmim][eFAP]) (Zhang *et al.*, 2008), CO_2 + 1-butyl-3-methylimidazolium acetate ([bmim][Ac]) (Shiflett *et al.*, 2008). A comparison between the solubility of CO_2 in the studied ionic liquids and these published ionic liquids are made at 323.15 K and presented in Figure 4.7.

To study the effect of cation alkyl chain length, the imidazolium-based ionic liquids paired with the [Tf_2N^-] anion ([pmim][Tf_2N], [bmim][Tf_2N] and [hmim][Tf_2N]) are taken into consideration. A marginal increase in CO_2 absorption is observed with an increment in cation alkyl chain length, for example from 20.04 % mole fraction of CO_2 to 20.8 % mole fraction of CO_2 to 23.1 % mole fraction of CO_2 at 323.15 K and 13 bar in the case of propyl (n = 3), butyl (n = 4) and hexyl (n = 6), respectively. The order for the three ionic liquids with the [Tf_2N^-] anion on the solubility of CO_2 is arranged with different alkyl chain lengths as follows: [$hmim^+$] > [$bmim^+$] > [$pmim^+$]. It can be concluded that the solubility of CO_2 slightly increases with the cation alkyl chain length.
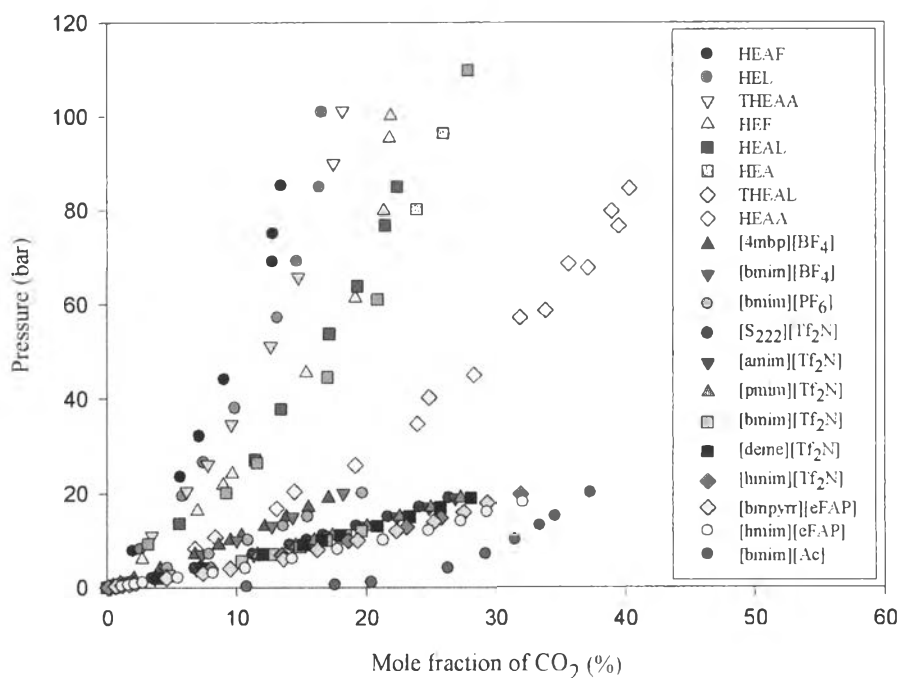
Figure 4.7 Comparison between the solubility of CO_2 in the studied ionic liquids and others published in the literature at 323.15 K: black ●, HEAF (Yuan *et al.* (2007)); red ●, HEL (Yuan *et al.* (2007)); green ▼, THEAA (Yuan *et al.* (2007)); yellow ▲, HEF (Yuan *et al.* (2007)); blue ■, HEAL (Yuan *et al.* (2007)); pink ■, HEA (Yuan *et al.* (2007)); cyan ♦, THEAL (Yuan *et al.* (2007)); gray ♦, HEAA (Yuan *et al.* (2007)); dark red ▲, [4mbp][BF₄] (this work); dark green ▼, [bmim][BF₄] (Shiflett and Yokozeki (2005)); dark yellow ●, [bmim][PF₆] (Shiflett and Yokozeki (2005)); dark blue ●, [S₂₂₂][Tf₂N] (this work); dark pink ▼, [amim][Tf₂N] (this work); dark cyan ▲, [pmim][Tf₂N] (this work); dark gray ■, [bmim][Tf₂N] (Anthony *et al.* (2005)); black ■, [deme][Tf₂N] (this work); red ♦, [hmim][Tf₂N] (Shiflett and Yokozeki (2007)); green ♦, [bmpyrr][eFAP] (Zhang *et al.* (2008)); yellow ●, [hmim][eFAP] (Zhang *et al.* (2008)); blue ●, [bmim][Ac] (Shiflett *et al.* (2008)).

As mentioned earlier, by changing the cation type from imidazolium- to pyridinium- based ionic liquids with the same anion has no difference in solubility of CO_2 (Yunus *et al.*, 2012). Comparing the cations [4mbp⁺] and [bmim⁺] paired

with the fixed anion [BF_4^-], the imidazolium ionic liquid [bmim][BF_4] presents slightly higher CO_2 absorption than the pyridinium ionic liquid [4mbp][BF_4]. At 323.15 K, the ionic liquid [bmim][BF_4] published by Shiflett and Yokozeki (2005) shows a solubility in mole fraction percent of 12.7 % at 13 bar and 14.3 % at 15 bar, while the ionic liquid [4mbp][BF_4] in this work shows the solubility of 12.16 % at 13 bar and 13.83 % at 15 bar. The results indicate comparable solubility values between ionic liquids consisting of imidazolium and pyridinium cations. Muldoon *et al.* reported that, at low pressures, there was very little difference in CO_2 solubility between the imidazolium and pyridinium cations (Muldoon *et al.*, 2007). Therefore, the ionic liquids containing imidazolium and pyridinium cations paired with a similar type of anion have an insignificant influence on the solubility of CO_2.

For all of ionic liquids based on the same [Tf_2N^-] anion ([S_{222}][Tf_2N], [amim][Tf_2N], [pmim][Tf_2N], [bmim][Tf_2N], [deme][Tf_2N], [hmim][Tf_2N]), it is noticeable that the solubility of CO_2 tends to decrease in the following manners: [hmim][Tf_2N] > [deme][Tf_2N] > [bmim][Tf_2N] > [pmim][Tf_2N] > [amim][Tf_2N] > [S_{222}][Tf_2N]. In summary, ionic liquids with the ammonium cation [deme][Tf_2N] have similar CO_2 capacity to [hmim][Tf_2N]; which demonstrates superior CO_2 solubility in terms of the physically CO_2-absorbing ionic liquid with the [Tf_2N^-] anion.

The effect of fluorination of anions can be explained by comparing the solubility of CO_2 in two sets of ionic liquids with the similar type of cations. The first set includes [hmim][Tf_2N] and [hmim][eFAP], and the second set includes [bmim][BF_4], [bmim][PF_6] and [bmim][Tf_2N]. Between [hmim][Tf_2N] and [hmim][eFAP], the comparison demonstrates that the solubility of CO_2 in [hmim][eFAP] is higher than the solubility in [hmim][Tf_2N]. For example, at the 10 bar pressure and 323.15 K , Zhang *et al.* reported that the solubility of CO_2 in [hmim][eFAP] as 21.3 mole % (Zhang *et al.*, 2008), and Shiflett and Yokozeki reported the solubility of CO_2 in [hmim][Tf_2N] was 18.6 % (Shiflett and Yokozeki, 2007). In case of [bmim][BF_4], [bmim][PF_6] and [bmim][Tf_2N], the results of the comparison indicate that the ionic liquid containing [Tf_2N^-] anion gives the highest CO_2 absorption compared to the ionic liquid containing [PF_6^-] and [BF_4^-] anions. The reported solubility of CO_2 in [bmim][BF_4] (Shiflett and Yokozeki, 2005),

[bmim][PF$_6$] (Shiflett and Yokozeki, 2005), and [bmim][Tf$_2$N] (Anthony *et al.*, 2005) at 13 bar and 323.15 K were 12.7, 13.6 and 20.8 %, respectively. In conclusion, an increase in the fluorination of the anions is likely to enhance the solubility of CO_2 in ionic liquids as shown in the following trend: [eFAP$^-$] > [Tf$_2$N$^-$] > [PF$_6^-$] > [BF$_4^-$].

Earlier, we have discussed the influence of the structure of cations and anions on the solubility of CO_2 in the five investigated ionic liquids. The absorption of CO_2 in the ionic liquids tends to decrease due to the effect of the structural variation of the cations and anions in this sequence: [deme][Tf$_2$N] > [pmim][Tf$_2$N] > [amim][Tf$_2$N] > [S$_{222}$][Tf$_2$N] > [4mbp][BF$_4$]. The four ionic liquids ([deme][Tf$_2$N], [pmim][Tf$_2$N], [amim][Tf$_2$N] and [S$_{222}$][Tf$_2$N]) are deemed potential solvents for CO_2 capture because of high CO_2 solubility with physical absorption. These salts are competitive to the physically CO_2-absorbing ionic liquids presenting high CO_2 solubility such as [bmim][Tf$_2$N] (Anthony *et al.*, 2005), [hmim][Tf$_2$N] (Shiflett and Yokozeki, 2007) and [hmim][eFAP] (Zhang *et al.*, 2008). At 323.15 K and a range of pressures of 0.5, 1, 4 and 10 bar, the AADs of the CO_2 solubility in [deme][Tf$_2$N], [pmim][Tf$_2$N], [amim][Tf$_2$N], and [S$_{222}$][Tf$_2$N] compared to the solubility in [bmim][Tf$_2$N] are 3.4, 8.0, 11.1 and 13.3 %, respectively. In case of a comparison to [hmim][Tf$_2$N], the AADs of the CO_2 solubility are 7.3, 8.0, 10.2 and 12.5 %. The AADs of the solubility when compared with [hmim][eFAP] are 31.8, 35.0, 37.1 and 38.6 %. Based on the deviations presented above, we can ensure that the trend of the four investigated ionic liquids is [deme][Tf$_2$N] > [pmim][Tf$_2$N] > [amim][Tf$_2$N] > [S$_{222}$][Tf$_2$N]. Despite the lowest CO_2 solubility among the studied ionic liquids, the solubility of CO_2 in [4mbp][BF$_4$] is as high as the solubility in [bmim][BF$_4$] and [bmim][PF$_6$] which were reported by Shiflett and Yokozeki (2005). At 323.15 K and a range of pressures of 0.1, 0.5, 1, 4, 7, 10, 13 and 15 bar, the AADs of the CO_2 solubility in [4mbp][BF$_4$] and the solubility in [bmim][BF$_4$] and [bmim][PF$_6$] are 15.8 and 18.0 %.

Most of the contributions have provided information regarding the physical absorption of CO_2 in ionic liquids (Aki *et al.*, 2004; Baltus *et al.*, 2004; Shiflett and Yokozeki, 2005; Kim *et al.*, 2005; Kumełan *et al.*, 2006b; Kumełan *et al.*, 2006a; Lee and Outcalt, 2006; Shiflett and Yokozeki, 2007; Muldoon *et al.*,

2007; Kim *et al.*, 2007; Costa Gomes, 2007; Zhang *et al.*, 2008). As mentioned above, the four investigated ionic liquids (i.e., [deme][Tf$_2$N], [pmim][Tf$_2$N], [amim][Tf$_2$N], and [S$_{222}$][Tf$_2$N]) exhibit comparable CO_2 solubility to the ionic liquids with a similar [Tf$_2$N$^-$] anion. The evidence shows that the [Tf$_2$N$^-$] indicates high CO_2 solubility with physical absorption. Therefore, these ionic liquids are regarded as physical solvents. Despite the high physical CO_2 absorption of the four investigated ionic liquids compared to [bmim][Tf$_2$N], [hmim][Tf$_2$N] and [hmim][eFAP], it is obvious that the solubilities of CO_2 in the studied ionic liquids are much less than that in [bmim][Ac], which shows a highly unusual behavior in comparison to other ionic liquids as illustrated in Figure 4.7. According to Shiflett *et al.*, the possibility of the intermolecular chemical complex formations or chemical reactions was introduced to explain such unusual behavior (Shiflett *et al.*, 2008). The results from many analytical instruments confirm the presence of the chemical complex between CO_2 and [bmim][Ac]. So far, the ionic liquid [bmim][Ac] has apparently been the best ionic liquid providing the highest CO_2 solubility (chemical absorption) among other ionic liquids with physical absorption. Nonetheless, higher energy of regeneration is required due to the presence of the occurring chemical reactions and the chemical complex formations, which is similar to the CO_2 absorption using amines. According to Chowdhury *et al.*, the chemical complex forming between an amine and CO_2 is called "carbamate," and is a fairly stable salt. When the carbamate is formed, it takes an amount of heat energy to break the bonds and to regenerate the amines (Chowdhury *et al.*, 2011). Similar to those amines, heat of regeneration for the [bmim][Ac]-based CO_2 capture process is still essential to be applied even if there is a good possibility that IL-based CO_2 capture processes have a potential to be more energy-efficient (Shiflett *et al.*, 2010).

We have considered ammonium cations and compared the solubility of CO_2 in the studied ammonium-based ionic liquid [deme][Tf$_2$N] to other ionic liquids in the literature. As presented earlier, the highest CO_2 solubility in the ammonium-based ionic liquid [deme][Tf$_2$N] is reported among the studied ionic liquids. In Figure 4.7, [deme][Tf$_2$N] shows higher CO_2 solubility at 323.15 K than any other ammonium-based ionic liquids published by Yuan *et al.* (2007), which are HEAF, HEL, THEAA, HEF, HEAL, HEA, THEAL, HEAA. Figure 4.8 presents the

graphical representation of the comparison of the CO_2 solubility in [deme][Tf_2N] and the ammonium-based ionic liquids published by Kurnia *et al.* (2009), including 2-hydroxy-N-(2-hydroxyethyl)-N-methylethanaminium acetate (HHEMEA), 2-hydroxy-N-(2-hydroxyethyl)-N-methylethanaminium (HHEMEL), bis(2-hydroxyethyl)ammonium lactate (BHEAL), 2-hydroxyethanaminium lactate (HEL), bis(2-hydroxyethyl)ammonium acetate (BHEAA), 2-hydroxyethanaminium acetate (HEA) at 313.15 K. The comparison suggests that the ionic liquid [deme][Tf_2N] has the highest solubility of CO_2.
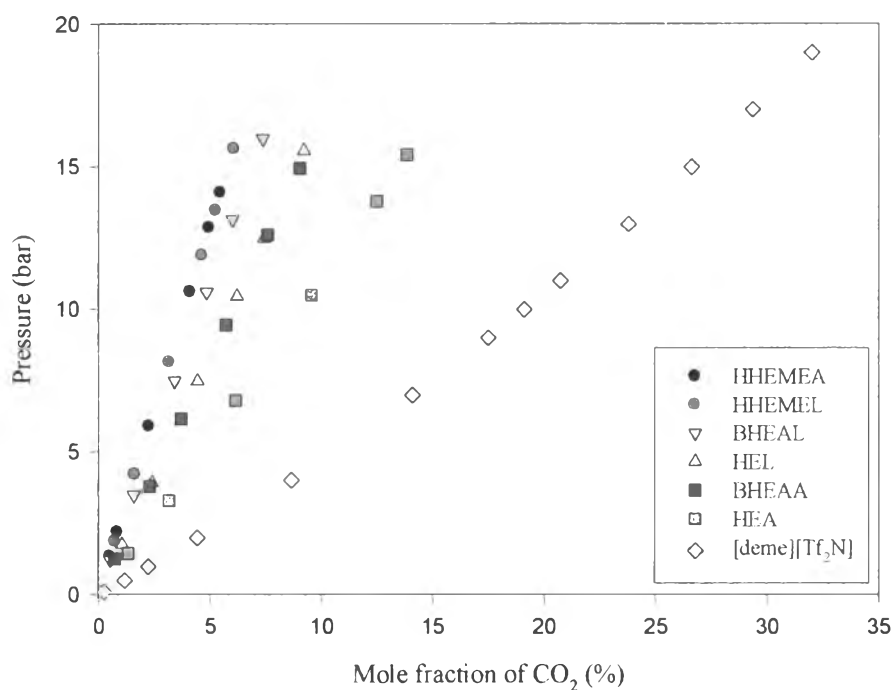
Figure 4.8 Comparison between the solubility of CO_2 in [deme][Tf_2N] and other ammonium-based ionic liquids in the literature at 313.15 K: black ●, HHEMEA (Kurnia *et al.* (2009)); red ●, HHEMEL (Kurnia *et al.* (2009)); green ▼, BHEAL (Kurnia *et al.* (2009)); yellow ▲, HEL (Kurnia *et al.* (2009)); blue ■, BHEAA (Kurnia *et al.* (2009)); pink ■, HEA (Kurnia *et al.* (2009)); cyan ♦, [deme][Tf_2N] (this work).

Moreover, we have made another comparison of the CO_2 solubility in [deme][Tf_2N] at 333.15 K with the existing ionic liquids which are composed of cations based on ammonium (Muldoon *et al.*, 2007) and phosphonium (Carvalho *et al.*, 2010), as shown in Figure 4.9. The published ammonium-based ionic liquids are N,N,N-trimethylbutylammonium bis(trifluoromethylsulfonyl)imide ([N_{4111}][Tf_2N]) and choline bis(trifluoromethylsulfonyl)imide ([choline][Tf_2N]), whereas the published phosphonium-based ionic liquid is trihexyltetra decylphosphonium bis(trifluoromethylsulfonyl)imide ([$P_{(14)666}$][Tf_2N]). The solubility of CO_2 in [deme][Tf_2N] presents slightly higher than those in [N_{4111}][Tf_2N] and [choline][Tf_2N]. For instance, at 333.15 K, the percentage mole fraction of CO_2 in [deme][Tf_2N] at 15 bar is 20.35 %, and that of CO_2 in [N_{4111}][Tf_2N] at 15.6 bar is 17.6%. In comparison to [choline][Tf_2N], the percentage mole fraction of CO_2 in [deme][Tf_2N] at 11 bar is 15.83 %, while that of CO_2 in [choline][Tf_2N] at 12 bar is 15.6 %. Even though [N_{4111}][Tf_2N] and [choline][Tf_2N] are measured at slightly higher pressures, the solubility of CO_2 in [deme][Tf_2N] is higher. The comparison confirms that there is a trivial difference between the solubility of CO_2 in [deme][Tf_2N] and those in [N_{4111}][Tf_2N] and [choline][Tf_2N] at low pressures up to 20 bar. We also compared the solubility of CO_2 in [deme][Tf_2N] with the phosphonium ionic liquid [$P_{(14)666}$][Tf_2N]. The graphical comparison illustrates that our ammonium-based ionic liquid [deme][Tf_2N] clearly exhibits significantly lower CO_2 solubility than [$P_{(14)666}$][Tf_2N].

In summary, the ionic liquid with the ammonium cation [deme][Tf_2N] is seemingly the most promising physical solvent for CO_2 capture among our studied ionic liquids. We have found that the order of the solubility of CO_2 in the five studied ionic liquids is [deme][Tf_2N] > [pmim][Tf_2N] > [amim][Tf_2N] > [S_{222}][Tf_2N] >> [4mbp][BF_4]. The explanation on their solubility has been discussed previously in detail. There is a potential feasibility for these ionic liquids to be used as green solvents because of competitively high CO_2 solubility to other physical ionic liquids. However, the CO_2 solubility investigations in these ionic liquids are limited at low pressure due to the limitation of the apparatus which can only be operated under 20 bar. The knowledge of high pressure solubility of these ionic liquids is necessary for further studies as well.
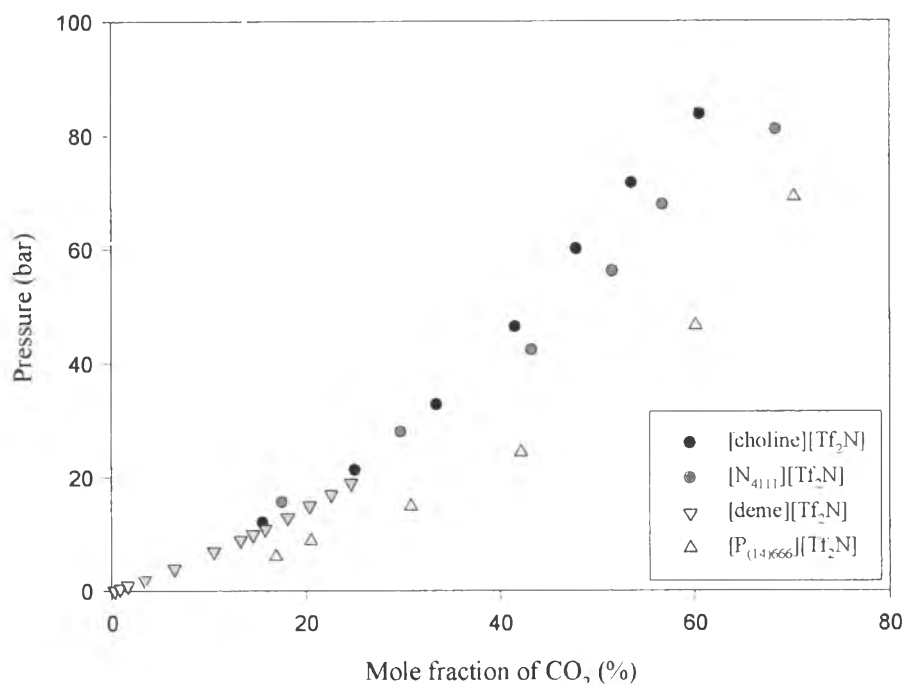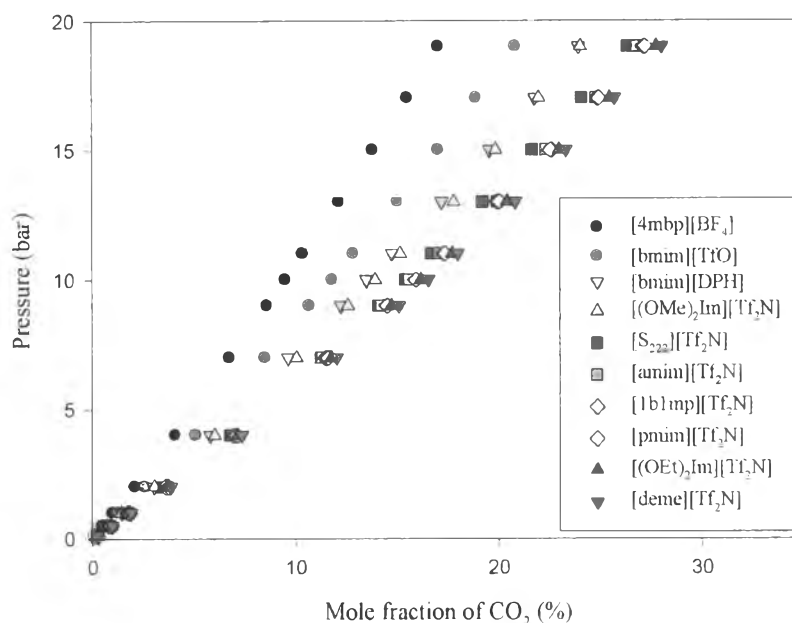
Figure 4.9 Comparison of the solubility of CO_2 in [deme][Tf_2N] with the existing ionic liquids containing ammonium and phosphonium cations in the literature at 333.15 K: black ●, [choline][Tf_2N] (Muldoon *et al.* (2007)); red ●, [N_{4111}][Tf_2N] (Muldoon *et al.* (2007)); green ▼, [deme][Tf_2N] (this work); yellow ▲, [$P_{(14)666}$][Tf_2N] (Carvalho *et al.* (2010)).

4.2.4 Comparison with Ionic Liquids in Our Group

In Figure 4.10, the comparison of the CO_2 solubility in [S_{222}][Tf_2N], [deme][Tf_2N], [pmim][Tf_2N], [amim][Tf_2N], and [4mbp][BF_4] was made at 323.15 K with the ionic liquids in our group, including 1-butyl-3-methylimidazolium trifluoromethanesulfonate ([bmim][TfO]), 1-butyl-3-methylimidazolium dibutyl phosphate [bmim][DPH], 1,3-dimethoxyimidazolium bis(trifluoromethyl-sulfonyl)imide ([(OMe)$_2$Im][Tf_2N]), 1-butyl-1-methylpiperidinium bis(trifluoromethylsulfonyl)imide ([1b1mp][Tf_2N]), and 1,3-diethoxyimidazolium bis(trifluoromethylsulfonyl)imide ([(OEt)$_2$Im][Tf_2N]) (Uygur, 2013). It is evident that the ammonium-based ionic liquid [deme][Tf_2N] in this work exhibit the highest CO_2 absorption among the ionic liquids in our group. The trend of the CO_2 solubility

is arranged in this order: [deme][Tf$_2$N] > [(OEt)$_2$Im][Tf$_2$N] > [pmim][Tf$_2$N] ≈ [1b1mp][Tf$_2$N] > [amim][Tf$_2$N] > [S$_{222}$][Tf$_2$N] > [(OMe)$_2$Im][Tf$_2$N]) > [bmim][DPH] > [bmim][TfO] > [4mbp][BF$_4$].

Figure 4.10 Comparison of the solubility of CO$_2$ in ionic liquids studied in our group at 323.15 K: black ●, [4mbp][BF$_4$] (this work); red ●, [bmim][TfO] (Uygur (2013)); green ▼, [bmim][DPH] (Uygur (2013)); yellow ▲, [(OMe)$_2$Im][Tf$_2$N] (Uygur (2013)); blue ■, [S$_{222}$][Tf$_2$N] (this work); pink ■, [amim][Tf$_2$N] (this work); cyan ♦, [1b1mp][Tf$_2$N] (Uygur (2013)); gray ♦, [pmim][Tf$_2$N] (this work); dark red ▲, [(OEt)$_2$Im][Tf$_2$N] (Uygur (2013)); dark green ▼, [deme][Tf$_2$N] (this work).

4.3 Thermodynamic Modeling

4.3.1 Critical Property Estimation

We have determined the normal boiling temperatures (T$_b$), the critical properties (T$_c$, P$_c$, and V$_c$), and the acentric factors (ω) of the five investigated ionic liquids to examine the binary interaction parameters for the equations of state and the activity coefficient model. The properties of CO$_2$ are easily obtained and widely

available. However, the properties of ionic liquids are not available and difficult to measure experimentally. The extended group contribution method based on the concept of Lydersen, and Joback and Reid, which is called "the modified Lydersen-Joback-Reid" method, is used to estimate those properties of the ionic liquids. The reason why we select this method is because it was proven to give good results for molecules of high molecular weight. This method is relatively simple because it requires a basic knowledge of the structure of the molecule and its molecular weight (Valderrama and Robles, 2007). The calculated critical properties, normal boiling temperatures, and acentric factors of the ionic liquids [S$_{222}$]Tf$_2$N], [deme][Tf$_2$N], [pmim][Tf$_2$N], [amim][Tf$_2$N] and [4mbp][BF$_4$] are summarized in Table 4.4. The consistency test of the estimated critical properties is presented in Appendix C. In order to verify "the modified Lydersen-Joback-Reid" method for our ionic liquids, the densities are calculated. The predicted densities are within acceptable range of errors. The AADs for [S$_{222}$][Tf$_2$N], [deme][Tf$_2$N], [pmim][Tf$_2$N], [amim][Tf$_2$N] and [4mbp][BF$_4$] are 9.2, 2.9, 1.7, 0.6 and 3.4 %, respectively.

Table 4.4 Molecular weights, normal boiling temperatures, critical properties, and acentric factors of ionic liquids

Ionic liquids	MW (g/mol)	T$_b$ (K)	T$_c$ (K)	P$_c$ (bar)	V$_c$ (cm^3/mol)	ω
[S$_{222}$][Tf$_2$N]	399.39	797.5	1191.1	21.9	1046.6	0.1561
[deme][Tf$_2$N]	426.40	760.6	1080.5	23.5	1028.2	0.3915
[pmim][Tf$_2$N]	405.34	839.4	1259.1	30.0	933.0	0.2575
[amim][Tf$_2$N]	403.32	836.2	1266.8	31.2	919.4	0.2349
[4mbp][BF$_4$]	237.05	484.8	625.8	18.9	703.7	0.8924

4.3.2 Equations of State

Many thermodynamic models have been proposed for modeling the phase behavior of ionic liquid + CO$_2$ systems. In this study, we have correlated the data with several thermodynamic models available within the AspenPlus process

simulator. The experimental CO_2 solubility data were correlated using the well-known equations of state including the standard Peng-Robinson (PR-EoS), the standard Redlich-Kwong-Soave (SRK-EoS), and the Redlich-Kwong-Soave (SRK) with quadratic mixing rules. The attractive and repulsive parameters required by the equations of state for a mixture are calculated from the pure component values using mixing rules. The adjustable binary interaction parameters, which characterize the interactions between unlike molecular species, were optimized by minimizing residual root mean square error.

4.3.2.1 The Standard Peng-Robinson (PR-EoS)

In case of the correlation with the standard PR-EoS, the binary interaction parameters (k_{12}) from 313.15 to 333.15 K for each system are given in Table 4.5. A linear function of k_{12} is fitted for each system as a function of temperature with minimized standard deviation. According to Enick *et al.*, the value of k_{12} for the standard PR-EoS can be either positive or negative values. The explainable meaning of the small and positive value represents a system of small, nonpolar, nonreacting components. On the other hand, the negative value of k_{12} indicates the attractive forces due to H-bonding. At higher temperatures, the H-bonding forces become less significant, therefore resulting in the binary k_{12} approaching values close to zero (Enick *et al.*, 1998). The explanations are able to describe the values of kij presented in Table 4.5. The calculated results from the standard PR-EoS are illustrated in Figures 4.11-4.15 along with the experimental data for the binary systems ([S_{222}][Tf$_2$N] + CO_2), ([deme][Tf$_2$N] + CO_2), ([pmim][Tf$_2$N] + CO_2), ([amim][Tf$_2$N] + CO_2) and ([4mbp][BF$_4$] + CO_2), respectively. The comparison of isothermal solubility data of CO_2 in different ionic liquids at several studied temperatures coupled with the estimations by the standard PR-EoS is presented in Figure 4.16. Deviations between the experimental and predicted pressures are shown in Table 4.6. The AADs are calculated in percent at each temperature for different systems. The average values of the AAD % of [S_{222}][Tf$_2$N], [deme][Tf$_2$N], [pmim][Tf$_2$N], [amim][Tf$_2$N] and [4mbp][BF$_4$] are 2.3, 2.3, 1.9, 2.2 and 1.0 %, respectively. The ionic liquid [4mbp][BF$_4$] gives the lowest average AAD % among the investigated ionic liquids. Therefore, the standard PR-

EoS correlates the data in good agreement with the experimental data for [4mbp][BF$_4$]. It can be concluded that the use of the standard PR-EoS is acceptable for modeling the solubility of CO$_2$ in [S$_{222}$][Tf$_2$N], [deme][Tf$_2$N], [pmim][Tf$_2$N], [amim][Tf$_2$N], and [4mbp][BF$_4$] over a range of pressure up to 20 bar.

Table 4.5 Binary interaction parameters of the standard PR-EoS for the ionic liquids (1) + CO$_2$ (2) system

Ionic liquids	Binary interaction parameter	T (K)		
		313.15	323.15	333.15
[S$_{222}$][Tf$_2$N]	$k_{12} = -0.3960+[0.0012 \times T(K)]$	-0.0275	-0.0157	-0.0039
[deme][Tf$_2$N]	$k_{12} = -0.6592+[0.0018 \times T(K)]$	-0.0944	-0.0763	-0.0583
[pmim][Tf$_2$N]	$k_{12} = -1.7402+[0.0051 \times T(K)]$	-0.1525	-0.1018	-0.0511
[amim][Tf$_2$N]	$k_{12} = -0.4712+[0.0012 \times T(K)]$	-0.0860	-0.0737	-0.0614
[4mbp][BF$_4$]	$k_{12} = -0.3694+[0.0015 \times T(K)]$	0.0897	0.1043	0.1190
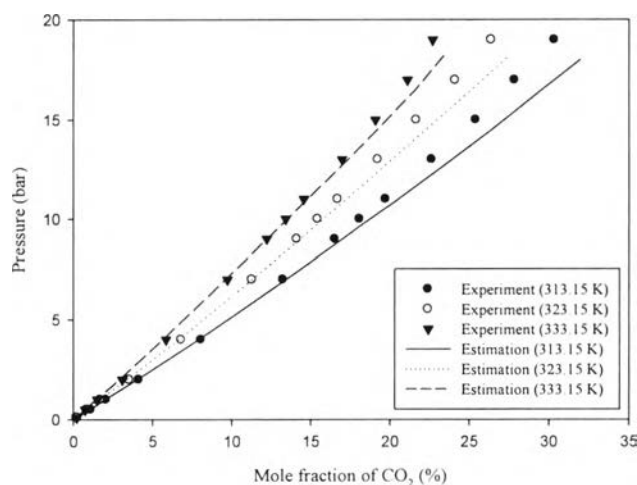
Figure 4.11 P-x diagram of the system [S$_{222}$][Tf$_2$N] and CO$_2$ for different temperatures. Symbols represent the experimental data: ●, at 313.15 K; ○, at 323.15 K; and ▼, at 333.15 K. Lines represent the estimations by the standard PR-EoS: solid line, at 313.15 K; dotted line, at 323.15 K; and dashed line, at 333.15 K.
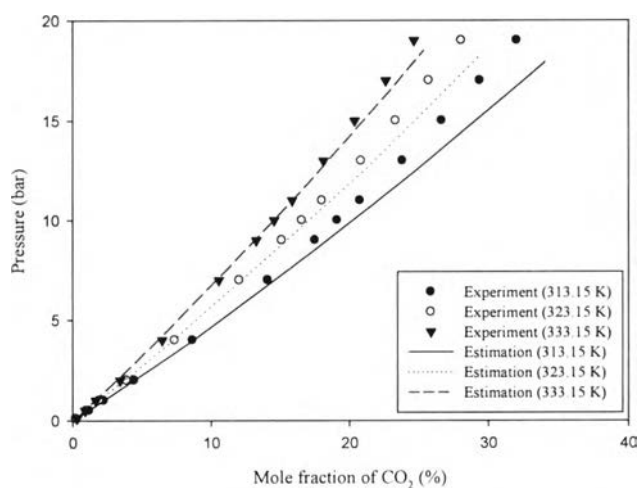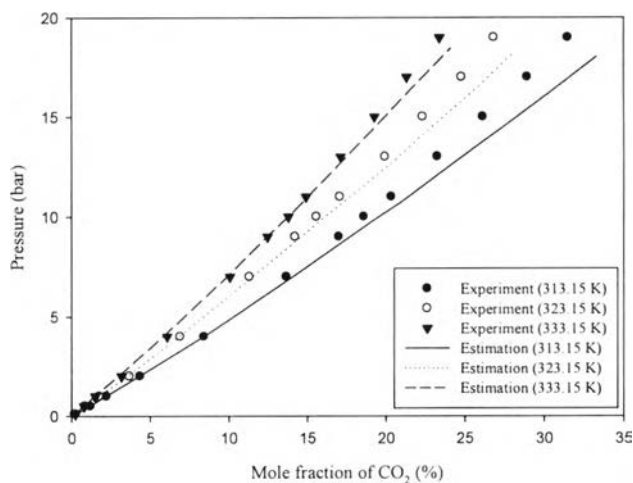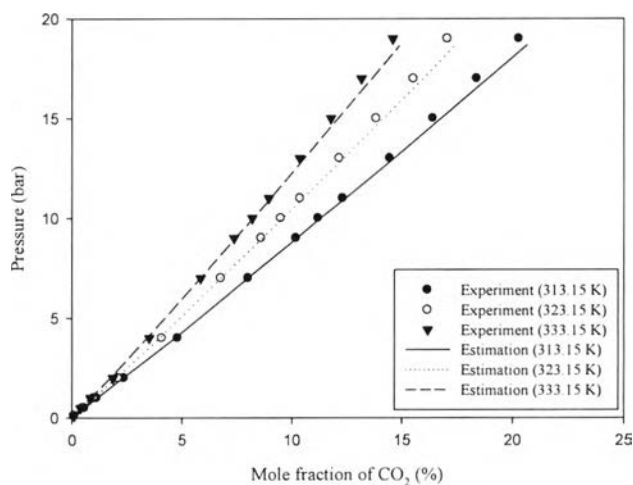
Figure 4.12 P-x diagram of the system [deme][Tf$_2$N] and CO$_2$ for different temperatures. Symbols represent the experimental data: ●, at 313.15 K; ○, at 323.15 K; and ▼, at 333.15 K. Lines represent the estimations by the standard PR-EoS: solid line, at 313.15 K; dotted line, at 323.15 K; and dashed line, at 333.15 K.
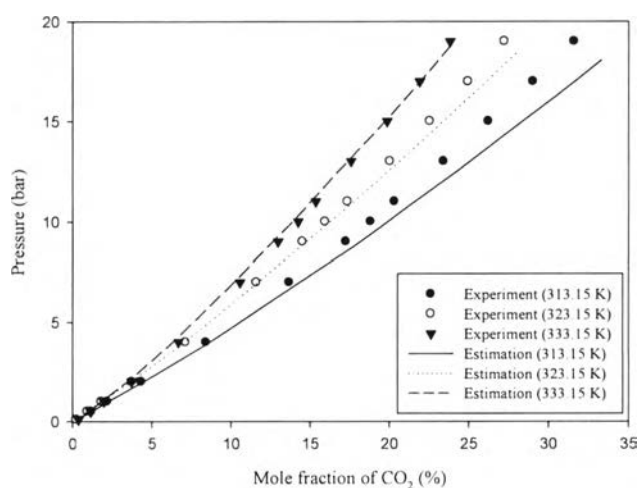

Figure 4.13 P-x diagram of the system [pmim][Tf$_2$N] and CO$_2$ for different temperatures. Symbols represent the experimental data: ●, at 313.15 K; ○, at 323.15 K; and ▼, at 333.15 K. Lines represent the estimations by the standard PR-EoS: solid line, at 313.15 K; dotted line, at 323.15 K; and dashed line, at 333.15 K.

Figure 4.14 P-x diagram of the system [amim][Tf$_2$N] and CO$_2$ for different temperatures. Symbols represent the experimental data: •, at 313.15 K; o, at 323.15 K; and ▼, at 333.15 K. Lines represent the estimations by the standard PR-EoS: solid line, at 313.15 K; dotted line, at 323.15 K; and dashed line, at 333.15 K.

Figure 4.15 P-x diagram of the system [4mbp][BF$_4$] and CO$_2$ for different temperatures. Symbols represent the experimental data: •, at 313.15 K; o, at 323.15 K; and ▼, at 333.15 K. Lines represent the estimations by the standard PR-EoS: solid line, at 313.15 K; dotted line, at 323.15 K; and dashed line, at 333.15 K.
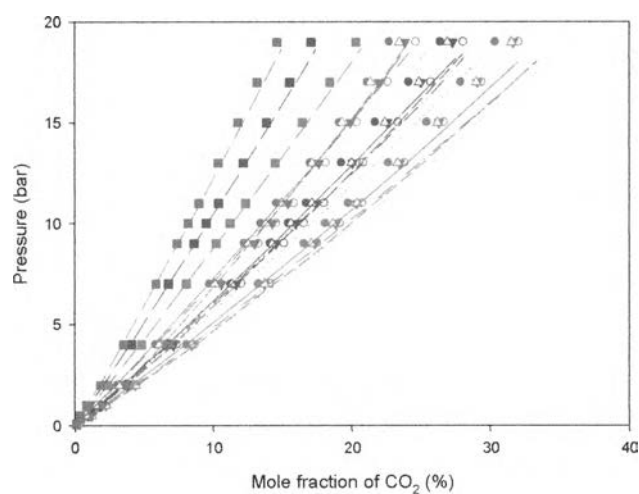
Figure 4.16 Comparison of isothermal solubility data of CO_2 in different ionic liquids: ●, $[S_{222}][Tf_2N]$; ○, $[deme][Tf_2N]$; ▼, $[pmim][Tf_2N]$; △, $[amim][Tf_2N]$; and ■, $[4mbp][BF_4]$; red, at 313.15 K; blue, at 323.15 K; and green, at 333.15 K. Lines represent the estimations by the standard PR-EoS.

Table 4.6 Average absolute deviation (AAD %) between experimental and estimated values of pressure by the standard PR-EoS for the ionic liquids + CO_2 system

| Ionic liquids	T (K)			
	313.15	323.15	333.15	Average
$[S_{222}][Tf_2N]$	2.5	1.9	2.3	2.3
$[deme][Tf_2N]$	2.5	2.1	2.5	2.3
$[pmim][Tf_2N]$	2.5	1.1	2.0	1.9
$[amim][Tf_2N]$	2.5	1.9	2.2	2.2
$[4mbp][BF_4]$	0.7	1.0	1.4	1.0

4.3.2.2 The Standard Redlich-Kwong-Soave (SRK-EoS)

We have also used the standard SRK-EoS to correlate the experimentally obtained solubility data of CO_2 in the studied ionic liquids. Table 4.7 shows the values of k_{12} at 313.15, 323.15 and 333.15 K for each ionic liquid + CO_2 system. Similarly, the binary interaction parameters are linearly expressed as a function of temperature. The P-x diagrams of each system are graphically presented for the experimental results and the calculated results from the standard SRK-EoS, as depicted in Figures 4.17-4.21. Figure 4.22 shows the experimental CO_2 solubility in different ionic liquids at different temperatures and the estimations by the standard SRK-EoS. The AADs between the experimental and predicted pressures at each temperature for different systems are also reported, including the average values, as shown in Table 4.8. The average values of AAD % of [S222][Tf2N], [deme][Tf2N], [pmim][Tf2N], [amim][Tf2N] and [4mbp][BF4] are 2.1, 2.2, 1.8, 2.1 and 1.0 %, respectively. Likewise, the ionic liquid [4mbp][BF4] had the lowest average AAD %. The averages of AAD % for the correlations with the standard SRK-EoS are comparable to the standard PR-EoS, but seem slightly lower. In conclusion, the standard SRK-EoS predicts better CO_2 solubility for our ionic liquid + CO_2 system than the standard PR-EoS.

Table 4.7 Binary interaction parameters of the standard SRK-EoS for the ionic liquids (1) + CO_2 (2) system

| Ionic liquids	Binary interaction parameter	T (K)		
		313.15	323.15	333.15
[S222][Tf2N]	$k_{12} = -0.4769+[0.0014 \times T(K)]$	-0.0383	-0.0243	-0.0103
[deme][Tf2N]	$k_{12} = -0.7731+[0.0021 \times T(K)]$	-0.1166	-0.0956	-0.0746
[pmim][Tf2N]	$k_{12} = -1.9412+[0.0056 \times T(K)]$	-0.1951	-0.1394	-0.0836
[amim][Tf2N]	$k_{12} = -0.5529+[0.0014 \times T(K)]$	-0.1107	-0.0966	-0.0824
[4mbp][BF4]	$k_{12} = -0.4469+[0.0017 \times T(K)]$	0.0854	0.1024	0.1194
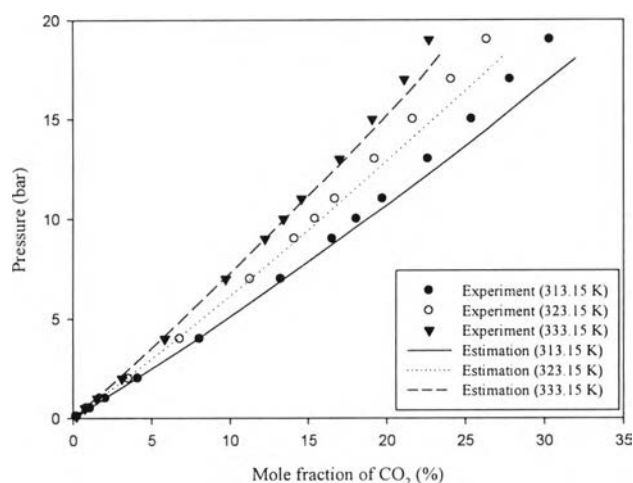
Figure 4.17 P-x diagram of the system $[S_{222}][Tf_2N]$ and CO_2 for different temperatures. Symbols represent the experimental data: ●, at 313.15 K; ○, at 323.15 K; and ▼, at 333.15 K. Lines represent the estimations by the standard SRK-EoS: solid line, at 313.15 K; dotted line, at 323.15 K; and dashed line, at 333.15 K.
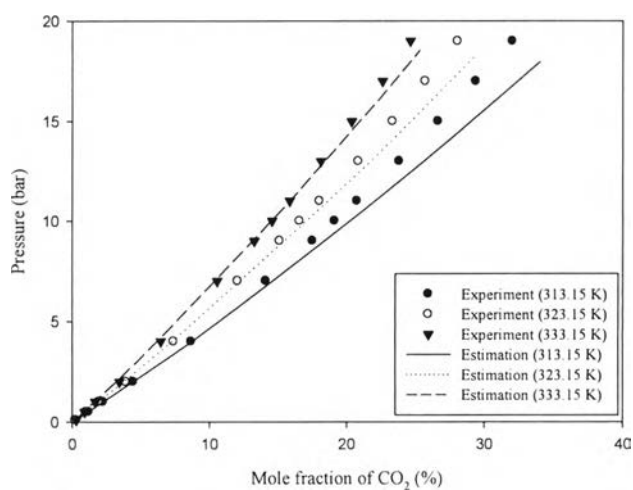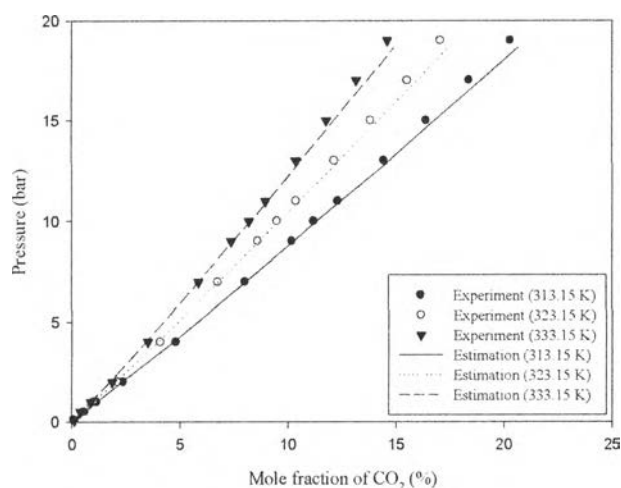

Figure 4.18 P-x diagram of the system [deme][Tf_2N] and CO_2 for different temperatures. Symbols represent the experimental data: ●, at 313.15 K; ○, at 323.15 K; and ▼, at 333.15 K. Lines represent the estimations by the standard SRK-EoS: solid line, at 313.15 K; dotted line, at 323.15 K; and dashed line, at 333.15 K.
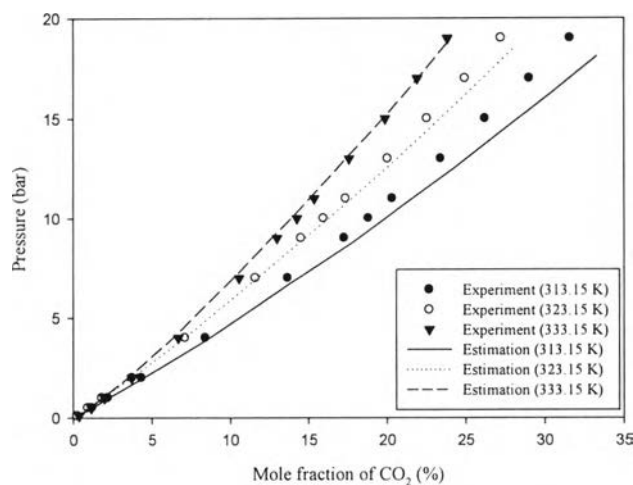
Figure 4.19 P-x diagram of the system [pmim][Tf$_2$N] and CO$_2$ for different temperatures. Symbols represent the experimental data: ●, at 313.15 K; ○, at 323.15 K; and ▼, at 333.15 K. Lines represent the estimations by the standard SRK-EoS: solid line, at 313.15 K; dotted line, at 323.15 K; and dashed line, at 333.15 K.
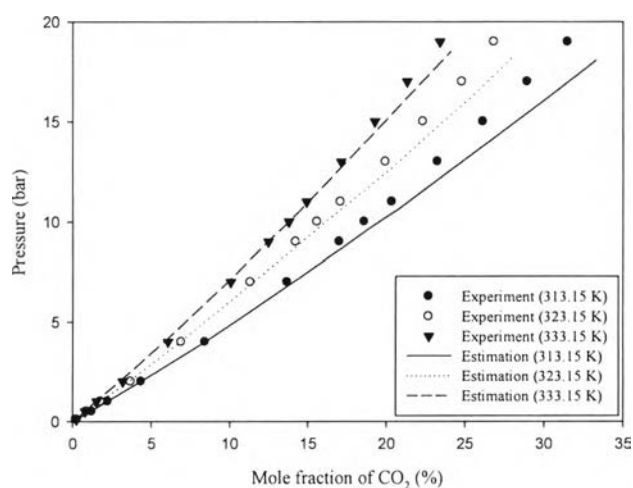

Figure 4.20 P-x diagram of the system [amim][Tf$_2$N] and CO$_2$ for different temperatures. Symbols represent the experimental data: ●, at 313.15 K; ○, at 323.15 K; and ▼, at 333.15 K. Lines represent the estimations by the standard SRK-EoS: solid line, at 313.15 K; dotted line, at 323.15 K; and dashed line, at 333.15 K.

Figure 4.21   P-x diagram of the system [4mbp][BF$_4$] and CO$_2$ for different temperatures. Symbols represent the experimental data: ●, at 313.15 K; ○, at 323.15 K; and ▼, at 333.15 K. Lines represent the estimations by the standard SRK-EoS: solid line, at 313.15 K; dotted line, at 323.15 K; and dashed line, at 333.15 K.
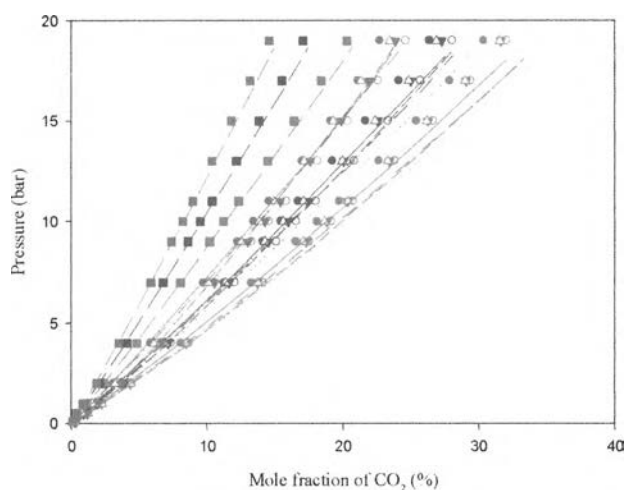
Figure 4.22   Comparison of isothermal solubility data of CO$_2$ in different ionic liquids: ●, [S$_{222}$][Tf$_2$N]; ○, [deme][Tf$_2$N]; ▼, [pmim][Tf$_2$N]; Δ, [amim][Tf$_2$N]; and ■, [4mbp][BF$_4$]; red, at 313.15 K; blue, at 323.15 K; and green, at 333.15 K. Lines represent the estimations by the standard SRK-EoS.

Table 4.8 Average absolute deviation (AAD %) between experimental and estimated values of pressure by the standard SRK-EoS for the ionic liquids + CO_2 system

Ionic liquids	T (K)			
	313.15	323.15	333.15	Average
$[S_{222}][Tf_2N]$	2.4	1.8	2.2	2.1
[deme][Tf_2N]	2.5	1.9	2.3	2.2
[pmim][Tf_2N]	2.6	1.0	1.8	1.8
[amim][Tf_2N]	2.4	1.8	2.1	2.1
[4mbp][BF_4]	0.8	1.0	1.4	1.0

*4.3.2.3 The Redlich-Kwong-Soave (SRK) with Quadratic Mixing Rules*

According to the evidence indicating the superior capability of the standard SRK-EoS over the standard PR-EoS in the case of the ionic liquid + CO_2 systems we dealt with in terms of lower average AADs, we have applied the quadratic mixing rules which are based on the two-interaction parameters k_{12} and l_{12} to the SRK-EoS. The mixing rules are adequate for mixtures containing polar components that are highly asymmetric with respect to size. The SRK with quadratic mixing rules can describe the experimental data of the solubility of CO_2 in $[S_{222}][Tf_2N]$, [deme][Tf_2N], [pmim][Tf_2N], [amim][Tf_2N] and [4mbp][BF_4]. The two binary interaction parameters (k_{12} and l_{12}) in the mixing rules are optimized using the experimental CO_2 solubility data. Table 4.9 summarizes the binary interaction parameters of the SRK with quadratic mixing rules at three different temperatures for each system. It is found that both k_{12} and l_{12} are a linear temperature-dependent function. Figures 4.23-4.27 shows the graphical representations of the modeling results and the experimental solubility for the ionic liquid + CO_2 systems. The comparison of the experimental results for five different ionic liquids at 313.15, 323.15 and 333.15 K along with the estimations by the SRK with quadratic mixing rules is presented in Figure 4.28. We have reported the AADs between the

experimental and correlated pressures in percent for each system and temperature. The AAD values are all less than 2 %, as shown in Table 4.10. The average values of AAD % of [S222][Tf2N], [deme][Tf2N], [pmim][Tf2N], [amim][Tf2N] and [4mbp][BF4] are 0.7, 1.0, 1.4, 0.9 and 0.6 %, respectively. For all of the equations of state used for modeling, the SRK with quadratic mixing rules can model the best the solubility of CO_2 in the studied ionic liquids [S222][Tf2N], [deme][Tf2N], [pmim][Tf2N], [amim][Tf2N] and [4mbp][BF4] at low pressure up to 20 bar and temperatures of 313.15, 323.15 and 333.15 K.

**Table 4.9** Binary interaction parameters of the SRK with quadratic mixing rules for the ionic liquids (1) + CO_2 (2) system

| Ionic liquids	Binary interaction parameters	T (K)		
		313.15	323.15	333.15
[S222][Tf2N]	$k_{12} = -0.1166 + [0.7001 \times T(K)/1000]$	0.1026	0.1096	0.1166
	$l_{12} = 0.0907 + [-0.1767 \times T(K)/1000]$	0.0353	0.0335	0.0318
[deme][Tf2N]	$k_{12} = 0.2111 + [-0.5112 \times T(K)/1000]$	0.0510	0.0459	0.0408
	$l_{12} = 0.1653 + [-0.4046 \times T(K)/1000]$	0.0386	0.0345	0.0305
[pmim][Tf2N]	$k_{12} = 1.1120 + [-3.2418 \times T(K)/1000]$	0.0968	0.0644	0.0319
	$l_{12} = 0.4607 + [-1.2867 \times T(K)/1000]$	0.0578	0.0449	0.0320
[amim][Tf2N]	$k_{12} = 0.0743 + [-0.1588 \times T(K)/1000]$	0.0246	0.0230	0.0214
	$l_{12} = 0.1293 + [-0.3063 \times T(K)/1000]$	0.0333	0.0303	0.0272
[4mbp][BF4]	$k_{12} = -1.2885 + [4.5123 \times T(K)/1000]$	0.1246	0.1697	0.2148
	$l_{12} = -0.2919 + [0.9775 \times T(K)/1000]$	0.0142	0.0240	0.0338
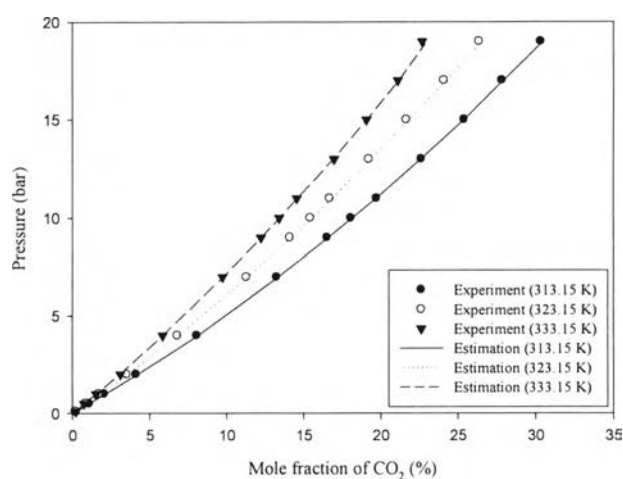
Figure 4.23 P-x diagram of the system [S$_{222}$][Tf$_2$N] and CO$_2$ for different temperatures. Symbols represent the experimental data: ●, at 313.15 K; ○, at 323.15 K; and ▼, at 333.15 K. Lines represent the estimations by the SRK with quadratic mixing rules: solid line, at 313.15 K; dotted line, at 323.15 K; and dashed line, at 333.15 K.
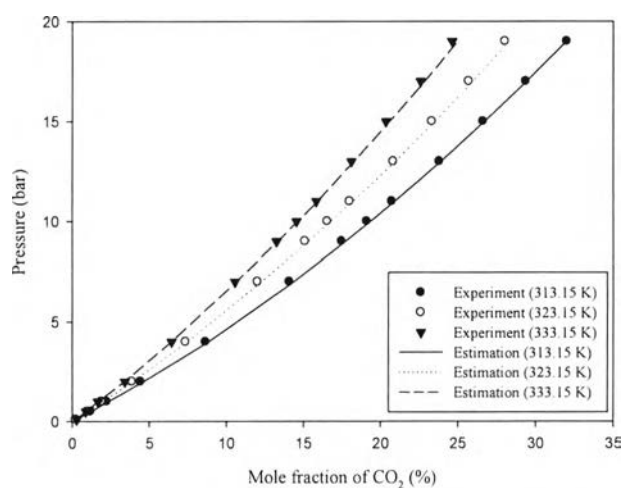
Figure 4.24 P-x diagram of the system [deme][Tf$_2$N] and CO$_2$ for different temperatures. Symbols represent the experimental data: ●, at 313.15 K; ○, at 323.15 K; and ▼, at 333.15 K. Lines represent the estimations by the SRK with quadratic mixing rules: solid line, at 313.15 K; dotted line, at 323.15 K; and dashed line, at 333.15 K.
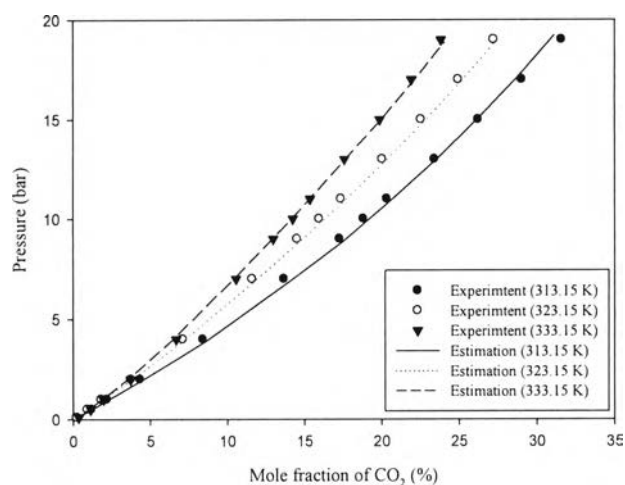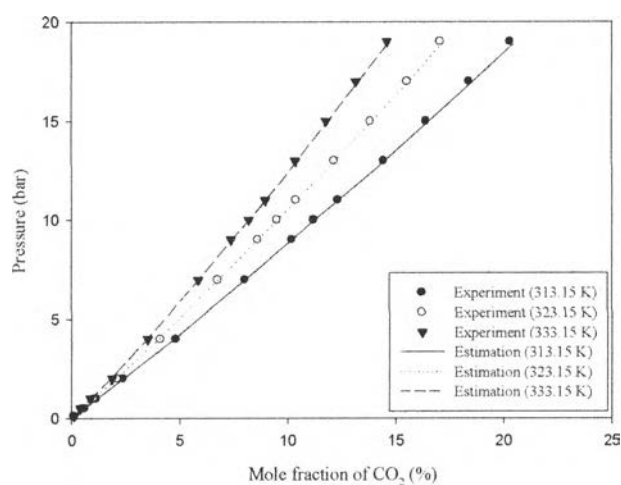
Figure 4.25   P-x diagram of the system [pmim][Tf$_2$N] and CO$_2$ for different temperatures. Symbols represent the experimental data: ●, at 313.15 K; ○, at 323.15 K; and ▼, at 333.15 K. Lines represent the estimations by the SRK with quadratic mixing rules: solid line, at 313.15 K; dotted line, at 323.15 K; and dashed line, at 333.15 K.
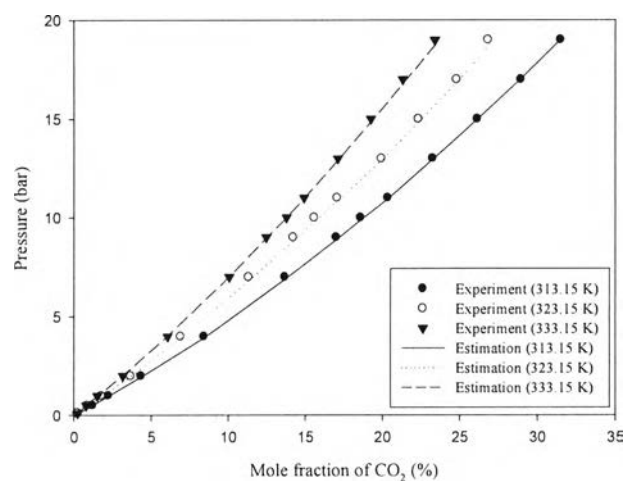

Figure 4.26   P-x diagram of the system [amim][Tf$_2$N] and CO$_2$ for different temperatures. Symbols represent the experimental data: ●, at 313.15 K; ○, at 323.15 K; and ▼, at 333.15 K. Lines represent the estimations by the SRK with quadratic mixing rules: solid line, at 313.15 K; dotted line, at 323.15 K; and dashed line, at 333.15 K.

Figure 4.27 P-x diagram of the system [4mbp][BF$_4$] and CO$_2$ for different temperatures. Symbols represent the experimental data: •, at 313.15 K; ○, at 323.15 K; and ▼, at 333.15 K. Lines represent the estimations by the SRK with quadratic mixing rules: solid line, at 313.15 K; dotted line, at 323.15 K; and dashed line, at 333.15 K.
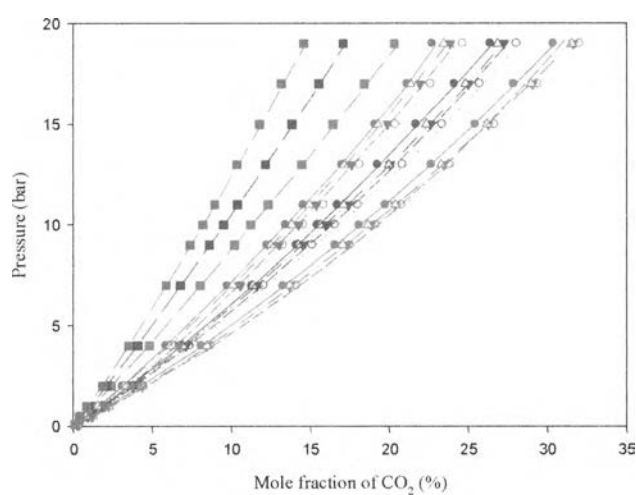
Figure 4.28 Comparison of isothermal solubility data of CO$_2$ in different ionic liquids: •, [S$_{222}$][Tf$_2$N]; ○, [deme][Tf$_2$N]; ▼, [pmim][Tf$_2$N]; Δ, [amim][Tf$_2$N]; and ■, [4mbp][BF$_4$]; red, at 313.15 K; blue, at 323.15 K; and green, at 333.15 K. Lines represent the estimations by the SRK with quadratic mixing rules.

Table 4.10 Average absolute deviation (AAD %) between experimental and estimated values of pressure by the SRK with quadratic mixing rules for the ionic liquids + CO_2 system

Ionic liquids	T (K)			
	313.15	323.15	333.15	Average
$[S_{222}][Tf_2N]$	0.6	0.7	0.7	0.7
[deme][Tf_2N]	1.0	0.9	1.2	1.0
[pmim][Tf_2N]	1.6	1.1	1.4	1.4
[amim][Tf_2N]	0.7	1.0	0.9	0.9
[4mbp][BF_4]	0.6	0.4	0.9	0.6

### 4.3.3 Activity Coefficient Model

4.3.3.1 The Non-Random Two-Liquid (NRTL)

Apart from the modeling using the equations of state, the well-known NRTL activity coefficient model is also used to correlate the solubility of CO_2 in our studied ionic liquids. Table 4.11 shows the binary interaction parameters adjusted to the experimental solubility data of the ionic liquids, which are $(g_{12}-g_{22})/R$ and $(g_{21}-g_{11})/R$. Both binary parameters are related to τ_{12} and τ_{21}, respectively. In this work, the parameter α was assumed to be a constant unique value of 0.3 in order to obtain more accurate results (Al-Rashed *et al.*, 2012). It is found that the binary interaction parameters for the NRTL model which are $(g_{12}-g_{22})/R$ and $(g_{21}-g_{11})/R$ can be linearly correlated as a function of temperature. The P-x diagrams of the ionic liquids + CO_2 mixture at three different temperatures are depicted in Figure 4.29-4.33. The comparison of isothermal solubility data of CO_2 in different ionic liquids in the range of studied temperatures coupled with the estimations by the NRTL is presented in Figure 4.34. The calculated pressures obtained from the NRTL are in good agreement with the experimental equilibrium pressures. VLE data are well-correlated by the NRTL activity coefficient model. The AADs from the experimental pressures presented in Table 4.12 are 0.7, 0.9, 1.3,

0.8 and 0.9 % for [S$_{222}$][Tf$_2$N], [deme][Tf$_2$N], [pmim][Tf$_2$N], [amim][Tf$_2$N] and [4mbp][BF$_4$], respectively. In conclusion, the NRTL as an activity coefficient model is capable of correlating very well for all the studied ionic liquids and CO$_2$ systems.

Table 4.11 Binary interaction parameters of the NRTL for the ionic liquids (1) + CO$_2$ (2) system ($\alpha = 0.3$)

| Ionic liquids	Binary interaction parameters	T (K)		
		313.15	323.15	333.15
[S$_{222}$][Tf$_2$N]	$(g_{12}-g_{22})/R = [-6.625\times T(K)]+1972.816$	-101.692	-167.939	-234.185
	$(g_{21}-g_{11})/R = [5.267\times T(K)]-1743.050$	-93.701	-41.032	11.638
[deme][Tf$_2$N]	$(g_{12}-g_{22})/R = [22.295\times T(K)]-7420.636$	-438.881	-215.929	7.024
	$(g_{21}-g_{11})/R = [-29.100\times T(K)]+9411.532$	298.872	7.872	-283.128
[pmim][Tf$_2$N]	$(g_{12}-g_{22})/R = [-47.842\times T(K)]+15947.450$	965.678	487.256	8.834
	$(g_{21}-g_{11})/R = [15.344\times T(K)]-5430.155$	-625.148	-471.707	-318.266
[amim][Tf$_2$N]	$(g_{12}-g_{22})/R = [-7.888\times T(K)]+2397.971$	-72.000	-150.875	-229.750
	$(g_{21}-g_{11})/R = [6.830\times T(K)]-2275.572$	-136.747	-68.447	-0.146
[4mbp][BF$_4$]	$(g_{12}-g_{22})/R = [-0.559\times T(K)]+305.191$	130.037	124.443	118.850
	$(g_{21}-g_{11})/R = [-0.580\times T(K)]+57.179$	-124.401	-130.199	-135.998
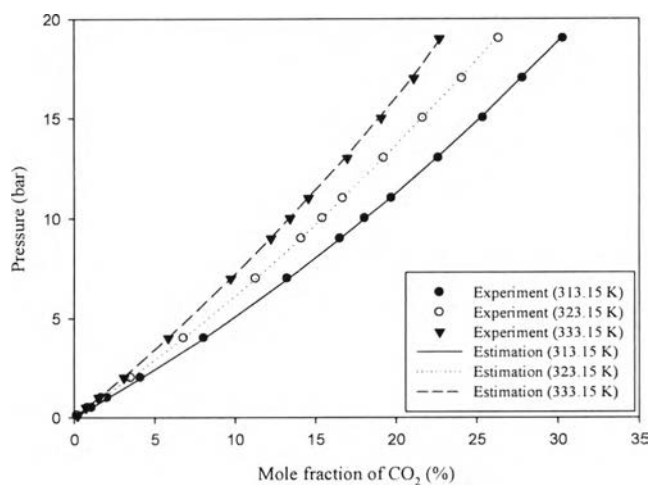
Figure 4.29 P-x diagram of the system $[S_{222}][Tf_2N]$ and CO_2 for different temperatures. Symbols represent the experimental data: ●, at 313.15 K; ○, at 323.15 K; and ▼, at 333.15 K. Lines represent the estimations by the NRTL: solid line, at 313.15 K; dotted line, at 323.15 K; and dashed line, at 333.15 K.
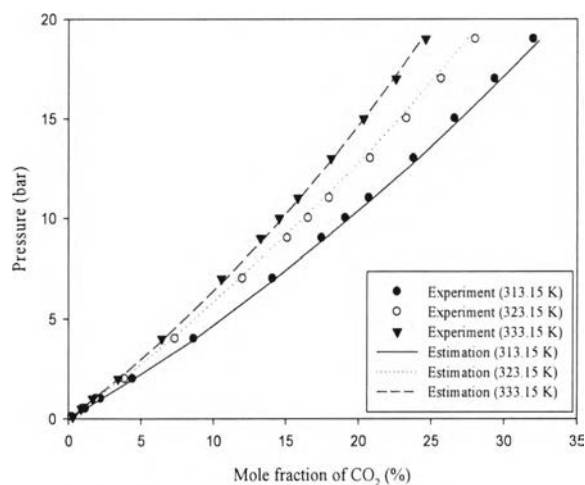
Figure 4.30 P-x diagram of the system [deme][Tf_2N] and CO_2 for different temperatures. Symbols represent the experimental data: ●, at 313.15 K; ○, at 323.15 K; and ▼, at 333.15 K. Lines represent the estimations by the NRTL: solid line, at 313.15 K; dotted line, at 323.15 K; and dashed line, at 333.15 K.
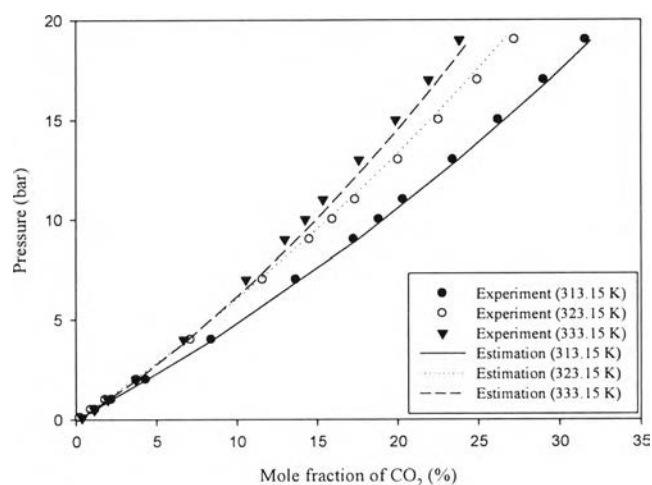
Figure 4.31 P-x diagram of the system [pmim][Tf$_2$N] and CO$_2$ for different temperatures. Symbols represent the experimental data: ●, at 313.15 K; o, at 323.15 K; and ▼, at 333.15 K. Lines represent the estimations by the NRTL: solid line, at 313.15 K; dotted line, at 323.15 K; and dashed line, at 333.15 K.
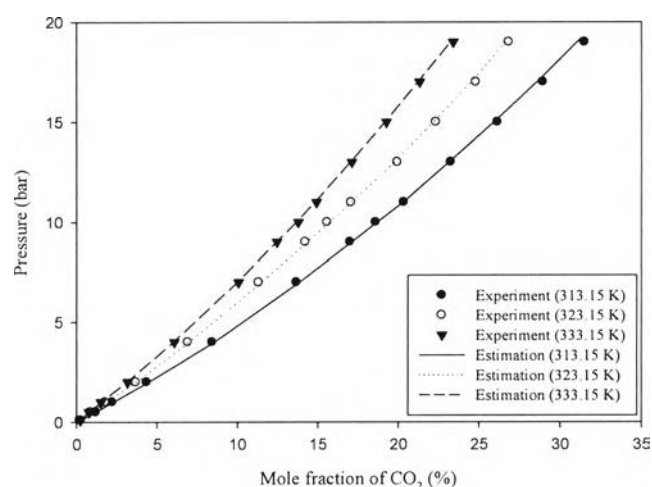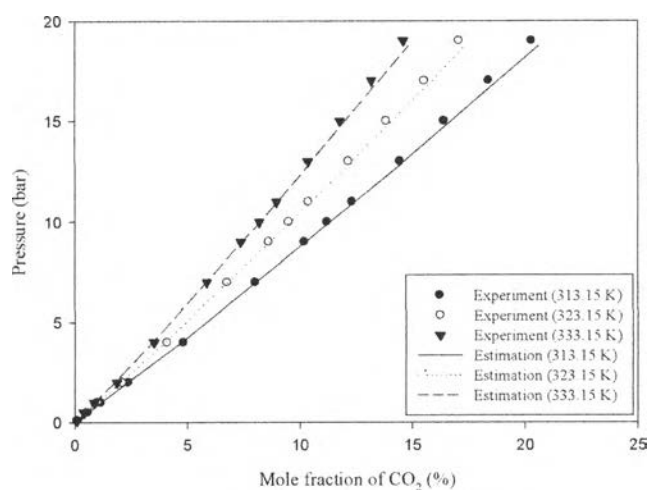

Figure 4.32 P-x diagram of the system [amim][Tf$_2$N] and CO$_2$ for different temperatures. Symbols represent the experimental data: ●, at 313.15 K; o, at 323.15 K; and ▼, at 333.15 K. Lines represent the estimations by the NRTL: solid line, at 313.15 K; dotted line, at 323.15 K; and dashed line, at 333.15 K.
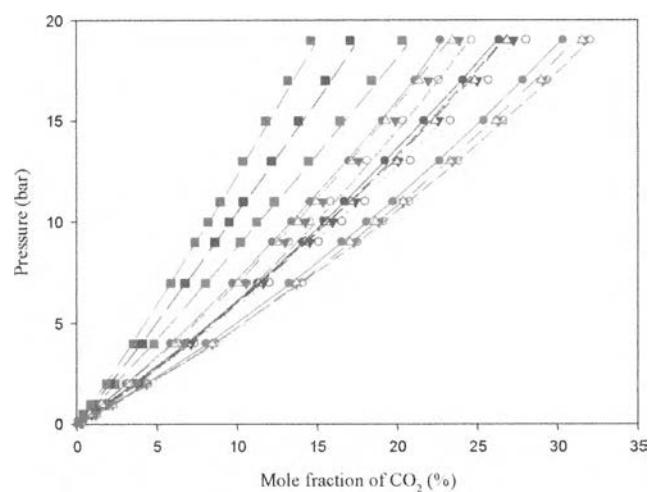
Figure 4.33 P-x diagram of the system [4mbp][BF₄] and CO₂ for different temperatures. Symbols represent the experimental data: ●, at 313.15 K; ○, at 323.15 K; and ▼, at 333.15 K. Lines represent the estimations by the NRTL: solid line, at 313.15 K; dotted line, at 323.15 K; and dashed line, at 333.15 K.

Figure 4.34 Comparison of isothermal solubility data of CO₂ in different ionic liquids: ●, [S₂₂₂][Tf₂N]; ○, [deme][Tf₂N]; ▼, [pmim][Tf₂N]; △, [amim][Tf₂N]; and ■, [4mbp][BF₄]; red, at 313.15 K; blue, at 323.15 K; and green, at 333.15 K. Lines represent the estimations by the NRTL.

Table 4.12 Average absolute deviation (AAD %) between experimental and estimated values of pressure by the NRTL for the ionic liquids + CO_2 system

ionic liquids	T (K)			
	313.15	323.15	333.15	Average
$[S_{222}][Tf_2N]$	0.5	0.5	1.0	0.7
$[deme][Tf_2N]$	0.3	1.4	0.9	0.9
$[pmim][Tf_2N]$	0.4	1.5	2.0	1.3
$[amim][Tf_2N]$	0.5	0.6	1.1	0.8
$[4mbp][BF_4]$	0.7	0.9	1.2	0.9

## 4.4 Henry's Law Constants and Enthalpies and Entropies of Absorption

4.4.1 Henry's Law Constants

According to the theory, a Henry's law constant has a linear relationship between gas concentration and pressure, which can be calculated from the slope of the experimental solubility data of gas at low solute concentrations. In most cases, the CO_2 isotherms are not linear over the whole range of pressures. Therefore, we fitted the experimental CO_2 solubility data with a second order polynomial and calculated the limiting slope as the pressure (or solubility) approaches zero (Anthony, 2004). In our research, we have estimated the fugacity coefficients from the experimental solubility data of the systems of the ionic liquids and CO_2 using the AspenPlus. The multiplication of the experimental pressure, mole fraction of CO_2 and fugacity coefficient provides the value of fugacity of CO_2. The plot of the fugacity of CO_2 versus the mole fraction of CO_2 at each temperature is reported in Appendix E. The Henry's law constant is found by fitting the data to a second order polynomial, which gives a correlation coefficient $R^2 > 0.999$. Considering the equilibrium conditions and infinite dilution, we took the limitation of the mole fraction of CO_2 approaching zero to obtain the Henry's law constant at each temperature.

Henry's law constants for CO_2 in our studied ionic liquids [S_{222}][Tf_2N], [deme][Tf_2N], [pmim][Tf_2N], [amim][Tf_2N], and [4mbp][BF_4] at three different temperatures are shown in Table 4.13. The graphical display of the Henry's law constants for CO_2 at all investigated temperatures is presented in Figure 4.35. We have found that the Henry's law constants at 313.15 K for all of the ionic liquid + CO_2 systems are smaller than those at other higher temperatures, indicating the temperature dependence of the solubility. With an increase in temperature, the solubility of CO_2 decreases. Hence, the Henry's law constant increases, for example, from 41.8 bar at 313.15 K to 56.9 bar at 333.15 K in case of [deme][Tf2N]. In comparison to the ionic liquids containing the [Tf_2N^-] anion, the insignificant differences in the Henry's law constants within these ionic liquids emphasize that the cations have little influence on the CO_2 solubility. The four ionic liquids with [Tf_2N^-] anion, [S_{222}][Tf_2N], [deme][Tf_2N], [pmim][Tf_2N], and [amim][Tf_2N], exhibit a relatively high affinity for CO_2 when compared to [4mbp][BF_4].

Table 4.13 Henry's law constants, enthalpies, and entropies of absorption for CO_2 in the studied ionic liquids

Ionic liquids	H (bar)			Δh (kJ/mol)	Δs (J/mol K)
	313.15 K	323.15 K	333.15 K		
[S_{222}][Tf_2N]	44.6	54.7	62.4	-14.6	-45.0
[deme][Tf_2N]	41.8	49.8	56.9	-13.4	-41.5
[pmim][Tf_2N]	43.3	52.5	55.1	-10.5	-32.5
[amim][Tf_2N]	43.8	54.3	60.8	-14.3	-44.2
[4mbp][BF_4]	82.7	97.1	111.5	-12.7	-40.2
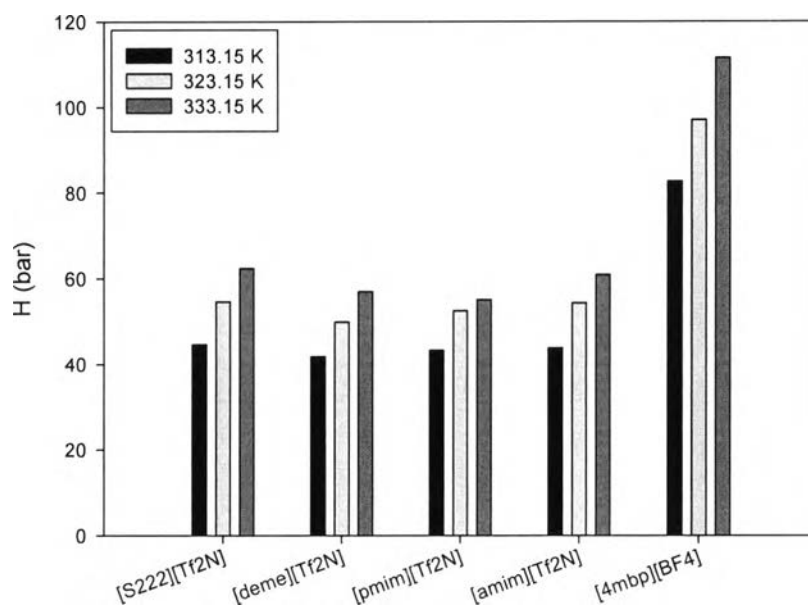
Figure 4.35 Henry's law constants for CO_2 in $[S_{222}][Tf_2N]$, $[deme][Tf_2N]$, $[pmim][Tf_2N]$, $[amim][Tf_2N]$ and $[4mbp][BF_4]$ at 313.15, 323.15 and 333.15 K.

Blath *et al.* (2011) have recently reported the Henry's law constant of CO_2 in $[S_{222}][Tf_2N]$ at 333.15 K, which was 66.9 bar Their result is consistent with the reported value of 62.4 bar in this work. The possible explanation for this difference in the Henry's law constant might be due to different amount of impurities in the ionic liquids. Blath *et al.* reported an overall purity of 99 % with water content of 1,837 ppm. Our ionic liquid also has a purity of 99 %, however, with water content less than 200 ppm.

4.4.2 Enthalpies and Entropies of Absorption

The dependence of the measured solubility of gases in the ionic liquids with temperature is pertaining to the thermodynamic properties of solvation, including the enthalpies (Δh) and entropies (Δs) of absorption. The enthalpy gives information regarding the strength of interaction between the liquid and the gas, while the entropy represents the level of ordering occurring in the ionic liquid/gas mixture (Anthony *et al.*, 2005; Galán Sánchez, 2008). According to the theory, the

enthalpy of absorption is obtained from the slope of the plot between the natural logarithm of the calculated Henry's law constant and the reciprocal inverse temperature (1/T) multiplied by the universal gas constant (8.314 J/mol K). On the other hand, the entropy of absorption is obtained from the product of the universal gas constant and the slope of the graph between the natural logarithm of the Henry's law constant and the natural logarithm of temperature. The plots are illustrated in Appendix E. As a consequence, the enthalpies and entropies of absorption require information about the solubility of gas at different temperatures. The enthalpy and entropy values for CO_2 in the studied ionic liquids [S_{222}][Tf_2N], [deme][Tf_2N], [pmim][Tf_2N], [amim][Tf_2N], and [4mbp][BF_4] are listed in Table 4.13. The highest enthalpy and entropy values for CO_2 in [S_{222}][Tf_2N] are Δh = -14.6 kJ/mol and Δs = -45.0 J/mol K, whereas the smallest values are Δh = -10.5 kJ/mol and Δs = -32.5 J/mol K for [pmim][Tf_2N]. The values for enthalpy and entropy of absorption are very comparable for all studied ionic liquids and relatively consistent with those published in the literature for absorption of CO_2 in [bmim][Tf_2N] (i.e., Δh = -11.4 kJ/mol and Δs = -37.6 J/mol K) and in [bmim][BF_4] (i.e., Δh = -15.9 kJ/mol and Δs = -52.4 J/mol K) (Anthony, 2004).

Concerning the physical meaning of the enthalpy and entropy of absorption, the strongest interaction between CO_2 and the ionic liquids corresponds to the most negative value of enthalpy of absorption. As observed, the negative enthalpies of absorption for all investigated ionic liquids indicate exothermic processes of absorption, which means that the absorptions of CO_2 in [S_{222}][Tf_2N], [deme][Tf_2N], [pmim][Tf_2N], [amim][Tf_2N], and [4mbp][BF_4] are favorable at lower temperatures. Moreover, the entropies of absorption indicate the increase of disorder in the absorption processes. It can be noted that the absorption of CO_2 decreases the order of the ionic liquids [S_{222}][Tf_2N], [deme][Tf_2N], [pmim][Tf_2N], [amim][Tf_2N], and [4mbp][BF_4]. In summary, it is evident that in all five investigated ionic liquids, there are significant interactions and ordering between the ionic liquids and CO_2 during the CO_2 absorption.